AFRL-AFOSR-VA-TR-2019-0228

Improving the Understanding of Heat and Carrier Transport in Electronic Heterostructure Devices by Proper Treatment of Boundary Effects in Wide Bandgap Structures including AlGaN

Mitra Dutta
UNIVERSITY OF ILLINOIS

08/05/2019
Final Report

Air Force Research Laboratory
AF Office Of Scientific Research (AFOSR)/ RTA1
Arlington, Virginia 22203
Air Force Materiel Command

REPORT DOCUMENTATION PAGE

Form Approved
OMB No. 0704-0188

1. REPORT DATE *(DD-MM-YYYY)*	**2. REPORT TYPE**	**3. DATES COVERED** *(From - To)*
02/08/2019	FINAL	15-07-2016 to 14-07-2019

4. TITLE AND SUBTITLE
Improving the Understanding Heat and Carrier Transport in High-Performance Electronic Heterostructure Devices through Proper Treatment of Boundary Effects in Wide Bandgap Structures including AlN-based and GaN-based Structures

5a. CONTRACT NUMBER

5b. GRANT NUMBER
AFOSR FA9550-16-1-0227

5c. PROGRAM ELEMENT NUMBER

6. AUTHOR(S)
Mitra Dutta

5d. PROJECT NUMBER

5e. TASK NUMBER

5f. WORK UNIT NUMBER

7. PERFORMING ORGANIZATION NAME(S) AND ADDRESS(ES)
Dept. of Electrical and Computer Engineering (MC 154)
Univ. of Illinois
851 S. Morgan Street, Chicago, IL 60607

8. PERFORMING ORGANIZATION REPORT NUMBER

9. SPONSORING/MONITORING AGENCY NAME(S) AND ADDRESS(ES)
AFOSR
4015 Wilson Blvd.
Arlington, VA 22203-1977

10. SPONSOR/MONITOR'S ACRONYM(S)

11. SPONSOR/MONITOR'S REPORT NUMBER(S)

12. DISTRIBUTION/AVAILABILITY STATEMENT
UNLIMITED DISTRIBUTION

13. SUPPLEMENTARY NOTES

14. ABSTRACT
This effort focuses on improving the fundamental understanding heat and carrier transport by better the modeling of phonons and phonon effects in electronic devices deals with the essential – but unimplemented – step of properly treating the full set of coupled phonon modes and boundary conditions at interfaces. In addition, this effort has considered LO phonon production from hot electrons that are accelerated form the 2DEG and eventually decay anharmonically into acoustic phonons which produce heat. Confinement effects have been taken into account in order to obtain correct LO phonon decay rates in dimensionally confined structures. In order to model transport in wurtzite structures – including AlN,

15. SUBJECT TERMS
III-V nitrides, interface phonons, heat transport, phonon engineering

16. SECURITY CLASSIFICATION OF:			**17. LIMITATION OF ABSTRACT**	**18. NUMBER OF PAGES**	**19a. NAME OF RESPONSIBLE PERSON**
a. REPORT	**b. ABSTRACT**	**c. THIS PAGE**			Mitra Dutta
					19b. TELEPHONE NUMBER *(Include area code)*
U	U	U	U	34	(312) 355-2131

FINAL TECHNICAL (Jul16-Jul19) REPORT ON

AFOSR FA9550-16-1-0227

"Improving the Understanding Heat and Carrier Transport in High-Performance Electronic Heterostructure Devices through Proper Treatment of Boundary Effects in Wide Bandgap Structures including AlN-based and GaN-based Structures"

ABSTRACT

The focus of this effort is on improving the fundamental understanding heat and carrier transport by better the modeling of phonons and phonon effects in electronic devices deals with the essential – but unimplemented – step of properly treating the full set of coupled phonon modes and boundary conditions at interfaces. In addition, this effort has considered LO phonon production from hot electrons that are accelerated form the 2DEG and eventually decay anharmonically into acoustic phonons which produce heat. Confinement effects have been taken into account in order to obtain correct LO phonon decay rates in dimensionally confined structures. In order to model transport in wurtzite structures – including AlN, GaN, and AlxGa1-xN – the known set of seven coupled differential equations describing the coupled mechanical (with acoustic content) and electrical (with optical content) phonon modes is being generalized by incorporation of anisotropic effects inherent in wurtzites such as GaN. The dielectric continuum model is being used to model interface phonon effects in these structures, including critical nanoscale confinement effects, and phonon scattering processes – including decay in dimensionally-confined structures – are being modeled based in consideration of anharmonic effects. These generalized equations are being applied to model slowness curves, dispersion curves, and transport rates using the full set of wurtzite (GaN-like and AlN-like) phonon-mode solutions of the above-described generalized equations. Experimental studies in this effort are aimed at verifying theoretical predictions. III-nitride superlattices have been characterized by Raman scattering.

(1) Introduction

The effort focusses on improving the understanding heat and carrier transport by improved modeling of phonons and phonon effects in electronic/optoelectronic devices deals with the essential – but unimplemented – step of properly treating the full set of coupled phonon modes and boundary conditions at interfaces. . In addition, this effort has considered LO phonon production from hot electrons that are accelerated form the 2DEG and eventually decay anharmonically into acoustic phonons which produce heat. Confinement effects have been taken into account in order to obtain correct LO phonon decay rates in dimensionally confined structures. In order to model transport in wurtzite structures – including AlN, GaN, and $Al_xGa_{1-x}N$ – the known set of seven coupled differential equations describing the coupled mechanical (with acoustic content) and electrical (with optical content) phonon modes is being generalized by incorporation of anisotropic effects inherent in wurtzites such as GaN. In addition, the dielectric continuum model is being used to model interface phonon effects in these structures, including critical nanoscale confinement effects, and phonon scattering processes – including decay in dimensionally-confined structures – are being modeled based in consideration of anharmonic effects. These generalized equations are being applied to model slowness curves, dispersion curves, and transport rates using the full set of wurtzite (GaN-like and AlN-like) phonon-mode solutions of the above-described generalized equations. These studies are incorporating nanoscale treatments of phonons and phonon effects near heterointerfaces. These studies will be complemented with selected experimental measurements to verify model predictions. III-nitride superlattices have been characterized by Raman scattering,

(2) List of Appendixes --- N/A

(3) Statement of Problem Studied

In order to improve the treatment of heat and carrier transport in GaN-based and AlN-based high-performance devices this effort considers coupled equations for phonon modes, confinement effects and anharmonic effects. To deal with the frequently-neglected – but important – (1) full set of boundary conditions, (2) coupling of mechanical (with acoustic content) and electrical (with optical content) modes, and (3) crystthsial anisotropy in a unified framework , we will to extend the very general treatment of Comas, Trallero-Giner and Cardona [1] by incorporating the anisotropy effects present in wurtzites – including AlN and GaN – using the uniaxial (where a c-axis is present) formulation of our past work on wurtzites [2-9]. With this anisotropic generalization of the treatment of Ref. 4, where the properly coupled acoustic and optical phonon modes are treated on a unified basis through coupled differential equations with accompanying boundary conditions, we are considering the thermal effects manifested by phonons at heterointerfaces. The formulation of Ref. 4 has been applied previously to

heterogeneous structures with two interfaces for the case where the bulk phonon description is no longer appropriate since the bulk phonon modes are replaced by confined phonons, interface phonons, and half-space phonons; see Ref. 3 for a description of these modes for zincblende and wurtzite crystals. However, it is essential to realize that even in the case of a single interface, the bulk phonons form interface phonons and half-space phonons. The interface and half-space phonons have been discussed extensively for the case of optical phonons (see Ref. 3 for references to many such papers, and Ref. 10 for a unifying treatment); however, there has been far less attention to such acoustic phonon modes. That such acoustic modes are present and important has been known for many years through the existence of Love acoustic waves, Rayleigh acoustic waves, Lamb acoustic waves, Stoneley acoustic waves, and coupled surface acoustic waves at interfaces; see Ref. 11 for an extensive discussion of such acoustic modes. Accordingly, our treatment of thermal effects near interfaces is based on the formulation of Ref. 4 with our incorporation of anisotropy. Importantly, the generality of this approach is enabling us to take into account the relevant interface and half-space modes near interfaces and to quantify their role in carrier and heat transport. In this effort, parallel studies on phonon-mediated carrier transport are based on the dielectric continuum model to study the effect of variations in phonon potentials on the nanoscale near interfaces. In addition, the dielectric continuum model and the elastic continuum model are used to incorporate confinement effects in essential processes such as anharmonic effects including phonon decay effects; these effects are being considered in both wurtzite and zincblende structures. These confinement and anharmonic effects are essential in the general application of the generalized seven coupled differential equations and their boundary conditions describing the coupled acoustic modes and the optical modes by including anisotropies so that these equations may be applied to anisotropic wurtzite crystals including GaN.

The basic formulation of Ref. 4 and an earlier paper by several authors of Ref. 4 [12] is being used in this effort. From Ref. 12, the equation of motion for the vibrational amplitude, u, which contains spatial dispersion, and coupling to the electrostatic field is the well-known equation,

$$\rho(\omega^2 - \omega_{TO}^2)\boldsymbol{u} - \boldsymbol{\nabla}(\rho v_a^2 \boldsymbol{\nabla}\cdot\boldsymbol{u}) - \nabla\cdot(\rho v_b^2 \boldsymbol{\nabla u}) + \left(\frac{(\epsilon_0 - \epsilon_\infty)}{4\pi}\right)^{1/2} \omega_{TO}\boldsymbol{E} = 0$$

where ρ is the mass per unit volume, ϵ_0 and ϵ_∞ are the static and high-frequency dielectric constants, and ω_{TO} is the bulk transverse-optical frequency.

Moreover, as from the forerunner of Ref. 4, Ref. 12, the mechanical forces have the form of the divergence of a tensor τ

$$\overleftrightarrow{\tau} = \rho v_a^2 \nabla\cdot\boldsymbol{u}\overleftrightarrow{I} + \rho v_b^2 \boldsymbol{\nabla u}$$

where $\boldsymbol{v_a}$ and $\boldsymbol{v_b}$ are related to the usual Lame constants λ and μ.

Based on this model, Ref. 12 examines how the mechanical and electrostatic fields can be obtained while taking their coupling fully into account. This coupling may be established within the context of electrostatics in terms of the electrostatic potential, Φ, the electric field, E, the displacement field, D, and the electric polarization, P, through,

$$\boldsymbol{E} = -\nabla\Phi, \quad \nabla \cdot \boldsymbol{D} = 0, \text{ and } \quad \boldsymbol{D} = \boldsymbol{E} + 4\pi\boldsymbol{P},$$

where, as is generally done, the external charge has been taken as zero as in Ref. 12.

Using the well-known constitutive relation of Born and Huang [13],

$$\mathbf{P} = \left(\frac{\rho(\epsilon_0 - \epsilon_\infty)}{4\pi}\right)^{1/2} \omega_{TO}\boldsymbol{u} + \frac{(\epsilon_\infty - 1)}{4\pi}\boldsymbol{E},$$

it follows that, from Ref. 12 that,

$$\nabla^2\Phi = 4\pi\, \boldsymbol{\nabla} \cdot \boldsymbol{P}.$$

Upon combining using the above expressions with the Lyddane-Sachs-Teller relations yields

$$\nabla^2\Phi = [4\pi\rho(\epsilon_\infty^{-1} - \epsilon_0^{-1})]^{1/2}\omega_{LO}\nabla \cdot \boldsymbol{u}.$$

The coupling between the u and Φ is now explicitly written into the field equations. In this way Ref. 12 illustrates the coupling between the mechanical (acoustic phonon variables) and electrostatic (optical phonon variables) by combining this last result with the initial equation for the vibrational mode amplitude above to yield:

$$\rho(\omega^2 - \omega_{TO}^2)\boldsymbol{u} - \boldsymbol{\nabla}(\rho v_a^2 \boldsymbol{\nabla} \cdot \boldsymbol{u}) - \nabla \cdot (\rho v_b^2 \boldsymbol{\nabla u}) - \left(\frac{(\epsilon_0 - \epsilon_\infty)}{4\pi}\right)^{1/2} \omega_{TO}\nabla\Phi = 0$$

The results of Ref. 12 are further extended and consolidated in Ref. 4 in a coherent and self-consistent manner based on a general Lagrangian approach. In particular, using this approach the results of Ref. 12 are extended by Ref. 4 to show that,

$$\rho\left(\omega^2 - {\omega_0}_j^2\right)u_j = \frac{\partial}{\partial x_l}\sigma_{jl} - \frac{i\omega}{c}\alpha_{jl}A_l + \alpha_{jl}\frac{\partial\phi}{\partial x_l},$$

$$\nabla^2 A_j + \frac{\omega^2}{c^2}\epsilon_{jl}^\infty A_l = -\frac{i\omega}{c}\left[\left(\epsilon_{jl}^\infty - \delta_{jl}\right)\frac{\partial\phi}{\partial x_l} - 4\pi\alpha_{jl}u_l\right],$$

and

$$\epsilon_{jl}^{\infty}\frac{\partial^2\phi}{\partial x_j\partial x_l}=\frac{i\omega}{c}\epsilon_{jl}^{\infty}\frac{\partial A_j}{\partial x_l}+4\pi\alpha_{jl}\frac{\partial u_j}{\partial x_l}$$

which constitute the set of seven second order coupled partial differential equations. In these equations, A is the vector potential, α_{jl}, is a tensor coupling the displacement with the electric field, σ_{jl} is the stress tensor, and all other quantities are as defined previously. In solving these coupled equations, as demonstrated in Ref. 4, it is necessary to require the continuity of u, A, φ, the normal component if the stress tensor, the tangential component of E, and the normal component of D.

It is the last set of three equations and the twelve accompanying boundary conditions that will be used in this research. However, to generalize this system so that it is applicable to wurtzite crystals – including GaN – it is necessary to follow the procedures that the co-authors employed in [3, 5-9] where the diagonal dielectric tensor is known to have one diagonal component corresponding to the c-axis dielectric and two equal diagonal components corresponding to the dielectric constant in the plane perpendicular to the c-axis. This generalization is being pursued in this research.

Experimental studies and theoretical modeling of the role interfaces on the carrier and thermal transport in structures including those in AlN-based and GaN-based devices as well as in wurtzite and zincblende structures generally are being undertaken in this research.

In this research we are considering particular AlN-based and GaN-based structures – as well as other wurtzite structures and zincblende structures - and we are modeling the role of interfaces on the carrier and thermal transport in structures including those in AlN-based GaN-based devices. Parallel studies on phonon-mediated carrier transport are being conducted using the dielectric continuum model to study the effect of variations in phonon potentials on the nanoscale near interfaces. Also as discussed previously, the dielectric continuum model and the elastic continuum model are being used to incorporate confinement effects in essential processes such as anharmonic effects including phonon decay effects; these effects will be considered in both wurtzite and zincblende structures.

Raman scattering measurements using the established UV-visible Raman measurement capabilities in the co-PI's NanoEngineering Research Laboratory are being used for: temperature profile measurements based the temperature dependence of the Raman modes as well as for essential measurements of phonon energies of the confined and interface phonons as well as the phonon linewidths for the determination of the essential phonon anharmonic decay rates as in our previously published papers.

(4) Summary of Most Important Results

The most important results obtained during this period of this effort include: determination of anharmonic phonon decay rates for the decay of confined phonons; formulation of equations describing coupled acoustic-optical phonon modes in wurtzites; determination of momentum and energy relaxation rates of hot electrons that are emitting optical phonons which subsequently decay into acoustic phonons, which carry heat; TEM and Raman characterization of AlN-GaN superlattices that are being pursued for enhanced acoustic phonon speeds; and phonon engineering of AlN-GaN superlattices that are being pursued for enhanced acoustic phonon speeds.

In this research, the role of phonon confinement on the anharmonic decay of an LO is analyzed. Anharmonic interactions describe the decay of phonon modes in via the Klemens channel [1]. The interaction Hamiltonian for three phonon process can be written as

$$H_{k,j;k',j';k'',j''} = \frac{1}{\sqrt{N}} P(k,j;k',j';k'',j'')\, u_{k,j} u_{k',j'} u_{k'',j''}$$

where k, k', k'' are the three phonon wave vectors involved in the annihilation or creation process, j, j', j'' are the polarization of the three phonons and N = number of unit cells present. P describes the cubic (anharmonic) coupling. The phonon displacement in normal coordinates is represented as:

$$u_{k,j} = \left(\frac{\bar{h}}{2m\omega_{k,j}}\right)^{\frac{1}{2}} e'_{k,j}\left(a_{k,j} e^{i\vec{k}\vec{r}} + a^{\dagger}_{k,j} e^{-i\vec{k}\vec{r}}\right)$$

$$u(\vec{r}) = \frac{1}{\sqrt{N}} \sum_{q} \sum_{j=1,2,3} \left(\frac{\bar{h}}{2m\omega_{q,j}}\right)^{\frac{1}{2}} \left(a_{q,j} e^{i\vec{q}\vec{r}} \widehat{e_{q,J}} + a^{\dagger}_{q,j} e^{-i\vec{q}\vec{r}} \widehat{e_{q,J}}^{\,*}\right) = \frac{1}{\sqrt{N}} \sum_{q} \sum_{j=1,2,3} \overrightarrow{u_{q,J}}$$

where $a_{k,j}$, $a^{\dagger}_{k,j}$ denoted the annihilation and creation operator, respectively, $e'_{k,j}$ is the polarization vector, m is the reduced mass of the lattice atoms and $\omega_{q,j}$ is the frequency of the normal mode. The displacement vector can be represented as following, with the direction of confinement and direction perpendicular to it.

$$u(\vec{r}) = e^{\pm i\vec{q}.\vec{r}} = u(z) e^{\pm i\overrightarrow{q_{II}}.\overrightarrow{r_{II}}} = \left(\cos(q_z z) \pm i sin(q_z z)\right) e^{\pm i\overrightarrow{q_{II}}.\overrightarrow{r_{II}}}$$

The decay lifetime for phonons can be calculated using Fermi golden rule, the matrix element in Fermi golden rule can be simplified as 1D problem for a quantum-confined structure confined in the z-direction.

$$\frac{1}{V}\int |M|^2{}_{ave}\,dV = \frac{1}{L_z}\int u^2(z)dz$$

Taking into account the confinement of the LO phonon in the GaAs structure to can be describe by either the slab model (V = 0 at $\pm\ L_z/2$) or the guided model (u = 0 at $\pm\ L_z/2$) [1] yields the same value for the average matrix element squared, respectively:

$$|M|^2{}_{ave} = \frac{1}{\pi}\int_{-\frac{\pi}{2}}^{\frac{\pi}{2}} \sin^2 y\,dy = \frac{1}{\pi}\int_{-\frac{\pi}{2}}^{\frac{\pi}{2}} \cos^2 y\,dy\ = \frac{1}{2}$$

These results indicate that the decay rate for the lowest LO phonon mode in either the slab or the guided model is approximately half that of the bulk phonon.

In this early period of the research we have also derived that describe the coupled acoustic-optical modes for wurtzites. We find,

$$\rho\ddot{u}_\imath - \gamma_{ij}u_j + \frac{\partial}{\partial x_j}\{\sigma_{ij}\} = -\alpha_{ij}E_j$$

Moreover, the polarization vector can be obtained as:

$$P_j = \alpha_{ij}u_i + \beta_{ij}E_i$$

The analytical expressions for β_{ij}, γ_{ij} and α_{ij} can also be obtained from the static and high frequency dielectric function of the medium. Explicit expressions for the full set of stress-strain relations for wurtzite crystals follow:

$$\left.\begin{aligned}
\sigma_{xx} &= c_{11}(u_{xx}+u_{yy}) + c_{13}u_{zz} - (c_{11}-c_{12})u_{yy} \\
\sigma_{yy} &= c_{11}(u_{xx}+u_{yy}) + c_{13}u_{zz} - (c_{11}-c_{12})u_{xx} \\
\sigma_{zz} &= c_{33}u_{zz} + c_{13}(u_{xx}+u_{yy}) \\
\sigma_{xy} &= (c_{11}-c_{12})u_{xy} \\
\sigma_{xz} &= 2c_{44}u_{xz} \\
\sigma_{yz} &= 2c_{44}u_{yz}
\end{aligned}\right\}$$

The carrier-phonon emission rates for momentum relaxation and energy relaxation were derived based on the Frohlich Hamiltonian [14]. These rates are depicted in Fig. 1. These rates

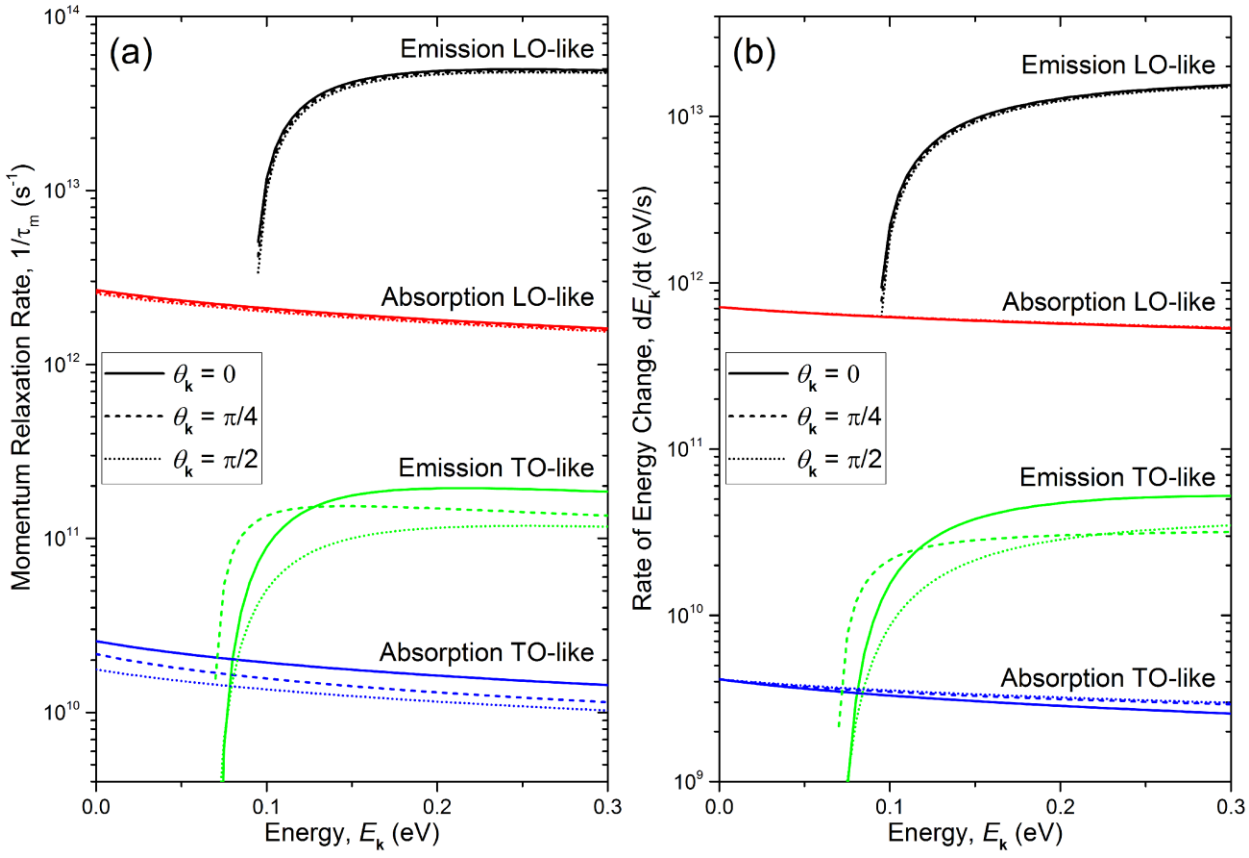

Fig. 1. (a) Absolute value of the momentum relaxation rates and (b) the rate of energy change due to emission and absorption of LO-like and TO-like phonons are plotted as a function of electron initial energy . The temperature is set to T = 300 K and the incident electron angles with respect to the c-axis are set to $\theta_k = 0$ (solid line), $\pi/4$ (dashed line), and $\pi/2$ (dotted line).

The size of the hot spot created when hot electrons emit optical phonons which in turn emit acoustic phonons that carry heat. Our initial estimated for the sizes of these hot spots are 10s on nm. In early efforts to engineer phonons to reduce the temperature of the hot, spot the high propagation velocity of interface (IF) optical has been estimated as compared with that of LO phonons in bulk. Since the IF optical phonon has a velocity roughly equal to that of an acoustic phonon, the IF optical modes propagate approximately 10 nm over their decay time with the consequence that the hot spot size is doubled from its nominal size of roughly 10 nm; this effect will lower the temperature of the hot spot. This focus will be explored further in the second year of this effort.

In another effort on engineering heat transport using phonon effects, the enhanced acoustic phonon velocity in superlattices is being examined. This approach depends on the growth of high-quality superlattices with little interface roughness; it is not yet clear that such superlattice quality is possible. Nevertheless, for high quality superlattices, the phonon velocity may be enhanced by replacing GaN with GaN-AlN superlattices where the relative thicknesses, d' and d, are those of the AlN layers and GaN layers in each superlattice period, respectively. Using an effective elastic constant mode we find that the sound speed of acoustic modes in the superlattice can be enhanced by about 30% as shown in Fig. 2.

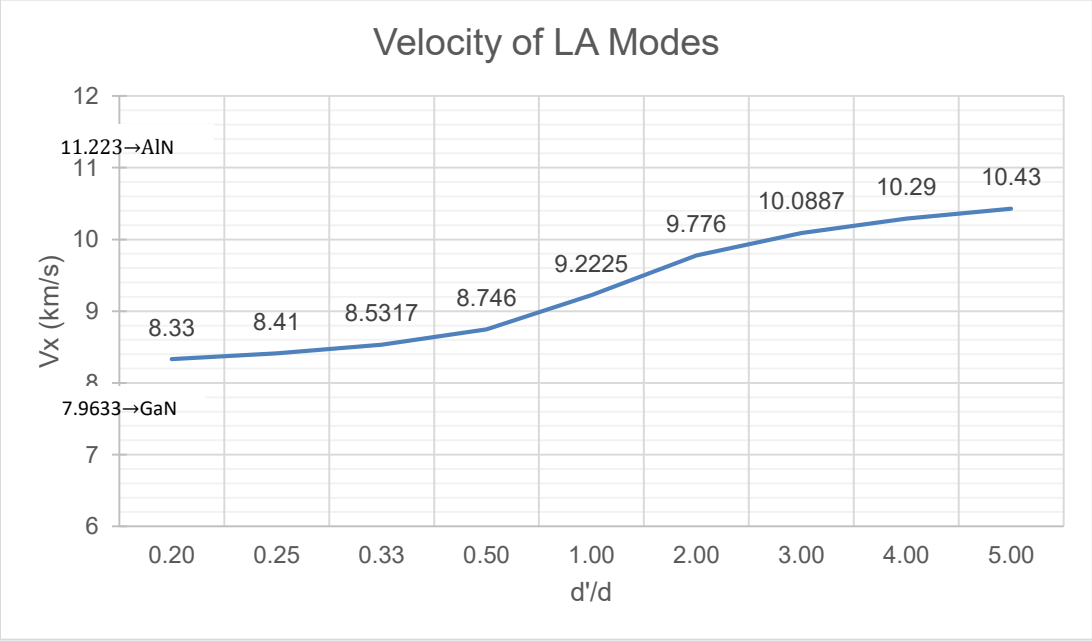

Fig. 2. Sound speed in an AlN-GaN superlattice as a function of the ratio, d'/d.

In this phonon engineering approach, the speed of the heat-carrying acoustic phonons is enhanced by about 30% as the Al-to-Ga content of the superlattice is enhanced. When piezoelectric stiffening is taken into account the results are as shown in Fig. 3.

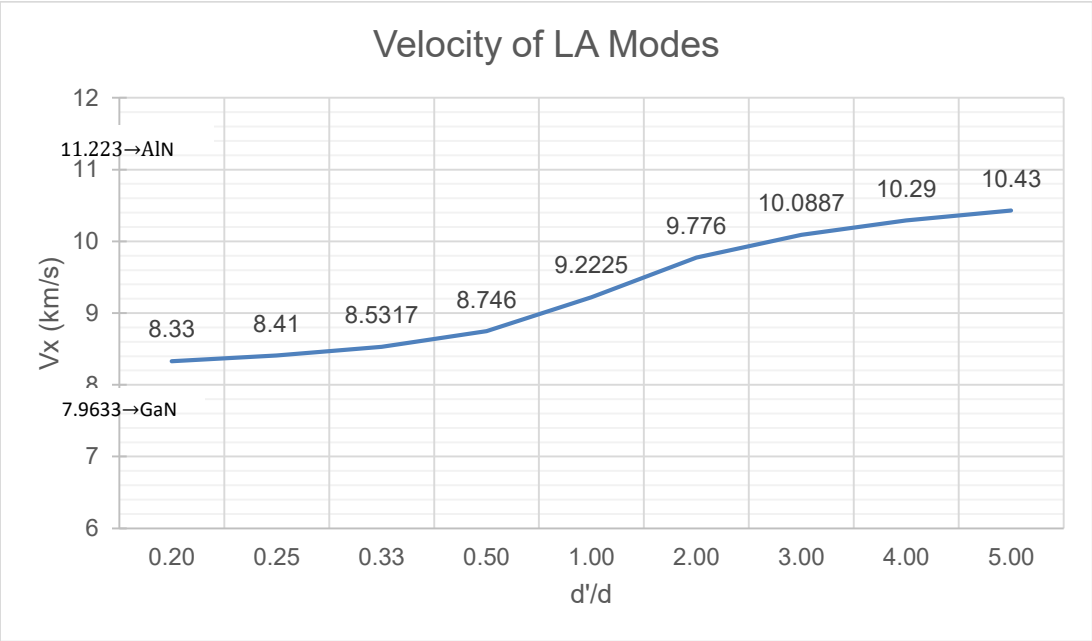

Fig. 3. Sound speed in an AlN-GaN superlattice as a function of the ratio, d'/d when piezoelectric stiffening is taken into account.

AlN-GaN superlattices with alternation layers that are 3 monolayers thick have been characterized using TEM; a TEM image is shown in Fig. 4.

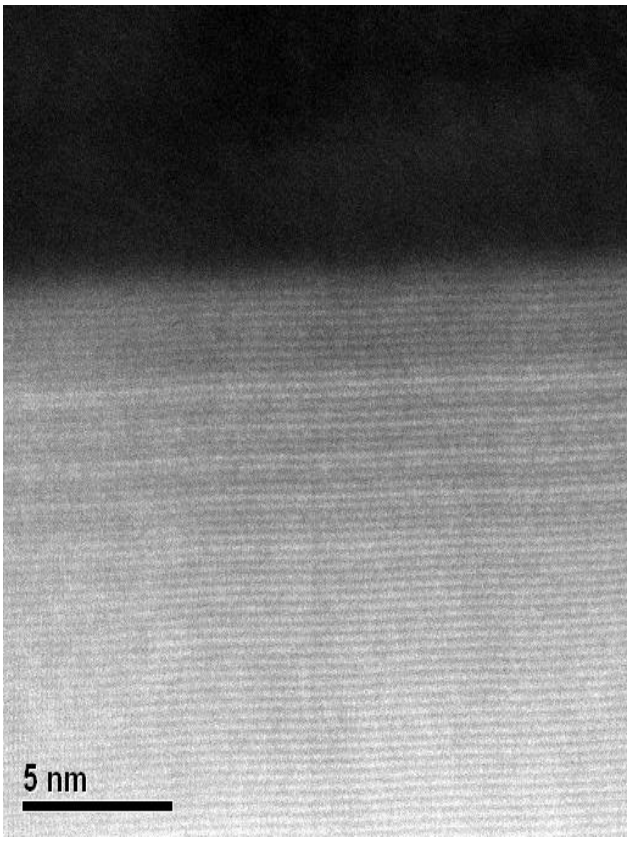

Fig. 4. TEM image of GaN-AlN superlattice having alternating layers that are 3 monolayers thick.

The superlattice of Fig. 4 corresponds to d'/d = 1 in Figs. 2 and 3.

Results from the first period of this effort include: determination of anharmonic phonon decay rates for the decay of confined phonons; formulation of equations describing coupled acoustic-optical phonon modes in wurtzites; determination of momentum and energy relaxation rates of hot electrons that are emitting optical phonons which subsequently decay into acoustic phonons, which carry heat; TEM and Raman characterization of AlN-GaN superlattices that are being pursued for enhanced acoustic phonon speeds; and phonon engineering of AlN-GaN superlattices that are being pursued for enhanced acoustic phonon speeds.

During this research, we have: determined the role of dimensional confinement on the lifetime of selected phonon modes; demonstrated that quantum wells may be realized that preferentially promote the emission of LO phonons in high-velocity interface phonon channels as opposed to lower-velocity confined phonons; demonstrated Raman-based techniques for measuring in semiconductors; and have made significant progress in understanding the basic coupling of optical

and acoustic phonons in dimensionally-confined wurtzite heterostructures. These advanced have been reported in:
Ketaki Sarkar, Debopam Datta, David J Gosztola, Fengyuan Shi, Alan Nicholls, Michael A Stroscio and Mitra Dutta, "Raman analysis of phonon modes in a short period AlN/GaN superlattice", Superlattices & Microstructures, 115, 116-122 (2018).

Debopam Datta, Mitra Dutta, and Michael A. Stroscio, 2017, July. Coupled acousto-optical phonons in wurtzites: Micro-to-nano-scale bridging. In Nanotechnology (IEEE-NANO), 2017 IEEE 17th International Conference on (pp. 189-192). IEEE. DOI: 10.1109/NANO.2017.8117416

Moreover, two additional key papers have been submitted as follows:

Debopam Datta, Kirupavathi Krishnababu, Michaal Stroscio, and Mitra Dutta, Effect of quantum confinement on lifetime of anharmonic decay of optical phonons in semiconductor nanostructures, Article reference: JPCM-111418 (submitted to Journal of Physics: Condensed Matter, June 2018)

Kihoon Park, Ahmed Mohamad, Can Bayram, Mitra Dutta, and Michael A. Stroscio, Electron Scattering via Interface Phonons with High Group Velocity in a Wurtzite GaN-based Quantum Well Structure, (submittted to Physical Review B, June 2018).

Additional portions of these results were reported in the peer-reviewed presentation:

Debopam Datta, Mitra Dutta, and Michael A. Stroscio, Coupled-Optical Phonons in Wurtzites: Micro-to-Nano-Scale Bridging, IEEE NANO 2017, Pittsburgh (July 2017).

More specifically, during this period, we have performed a detailed theoretical analysis and comparison of the interaction between electrons and optical phonons of interface and confined modes in a wurtzite AlN/GaN/AlN quantum well heterostructure based on the uniaxial dielectric continuum model. The formalism describing the interface and confined mode optical phonon dispersion relation, the electron–phonon scattering rates, and the average group velocity of emitted optical phonons were developed and numerically calculated. We have shown that the dispersion relation of the interface mode phonons shows a convergence of the symmetric and asymmetric modes to the resonant phonon frequencies 577.8 and 832.3 cm^{-1} with a steep slope around the zone center indicating a large group velocity of the interface phonons. The maximum group velocity of the interface mode phonons is 138 km/s which is almost 20 times larger than that of the confined mode phonons. At the onset of interface phonon emission, the average group velocity is small due to the large contribution of confined and interface mode phonons with close-to-zero group velocity, but eventually increases up to larger values than the bulk GaN longitudinal acoustic mode

phonon propagation velocity along the wurtzite crystal *c*-axis [0001] (8 nm/ps). We have shown that by adjusting the thickness of the GaN in the double heterostructure, the average group velocity can be engineered to become larger than the propagation of acoustic phonons at a specific electron energy. This suggests that the high group velocity interface mode optical phonons can be exploited to remove heat more effectively and reduce junction temperatures in GaN-based heterostructures.

Our novel phonon engineering technique provides an innovative way of spreading region over which optical phonons emitted by hot electrons before they emit heat carrying acoustic phonons. It is thus clear for the first time that fundamental phenomena underlying phonon engineering of confined and interface phonons can provide a means of modifying temperature distributions and reduce peak temperatures in III-nitride heterostructures having large Frohlich interactions.

In the double heterostructure of interest in this work, which is a GaN quantum well sandwiched by two AlN layers (AlN/GaN/AlN), there exists four distinct classes of optical phonon modes: the interface, confined, half-space, and propagating modes as discovered by Dutta, Stroscio and coworkers (see Stroscio and Dutta, Phonons in Nanostructures, Cambridge University Press, 2001). Among these four optical phonon modes, the electrons that are confined in the GaN quantum well mostly interact with the interface and confined phonons; the effect of the half-space and propagating modes on the electrons is negligible in this system. Here, therefore, we consider the electron scattering with interface and confined mode optical phonons.

In a heterostructure configuration, the available optical phonon modes and the phonon frequencies for each mode are determined by the relation between the dielectric constant functions. The frequency-dependent dielectric functions parallel ε_z and perpendicular ε_t to the *z*-axis are given as:

$$\varepsilon_z(\omega) = \varepsilon_z^{\infty} \frac{\omega^2 - \omega_{Lz}^2}{\omega^2 - \omega_z^2} \tag{1}$$

$$\varepsilon_t(\omega) = \varepsilon_t^{\infty} \frac{\omega^2 - \omega_{Lt}^2}{\omega^2 - \omega_t^2} \tag{2}$$

where ω is the phonon frequency, ω_{Lz}, ω_z, ω_{Lt}, and ω_t are the characteristic frequencies of A_1(LO: longitudinal-optical), A_1(TO: transverse-optical), E_1(LO), and E_1(TO) optical phonon modes, respectively. For the AlN/GaN/AlN quantum well, two sets of material parameters are required such that we obtain four dielectric functions, namely ε_{1z}, ε_{1t}, ε_{2z}, and ε_{2t}, where the subscripts 1 and 2 indicate the GaN and AlN, respectively. With ω = 0, the Lyddane-Sachs-Teller relation is recovered and the static dielectric constants are obtained. Throughout this paper, we take the *z*-axis along the *c*-axis of the wurtzite crystal [0001] and perpendicular to the heterointerfaces.

The conditions imposed on the available interface mode optical phonon frequency are

$$\varepsilon_{1z}\varepsilon_{1t} > 0,\ \varepsilon_{2z}\varepsilon_{2t} > 0, \text{ and } \varepsilon_{1z}\varepsilon_{2z} < 0\,. \tag{3}$$

For confined modes, the conditions are

$$\varepsilon_{1z}\varepsilon_{1t} < 0 \text{ and } \varepsilon_{2z}\varepsilon_{2t} > 0\,. \tag{4}$$

The characteristic frequencies of the dielectric functions which define the phonon frequency ranges are indicated by vertical dashed lines. The interface phonons are allowed in two phonon frequency intervals, $(\omega_{1t}, \omega_{2z})$ and $(\omega_{1Lt}, \omega_{2Lz})$. Since the former (latter) interval corresponds to the TO (LO) phonon frequencies of GaN and AlN, we label the phonon modes that lie in this

frequency range as TO (LO) interface phonons. These intervals are indicated in the figure as red and blue shaded regions, respectively. Similarly, the confined phonons are allowed in two phonon frequency intervals, $(\omega_{1z}, \omega_{1t})$ and $(\omega_{1Lz}, \omega_{1Lt})$. The characteristic phonon frequencies associated with these intervals are from the TO and LO phonon frequencies of GaN, and hence we label them as TO confined and LO confined phonons. The TO and LO confined phonon frequency ranges are shown in the figure as green and magenta shaded regions, respectively.

The dispersion relations for the symmetric q_S^{IF} and asymmetric q_A^{IF} interface phonon modes are described by

$$q_S^{IF} = \frac{1}{2\alpha d}\ln\left[\frac{\xi_1+\xi_2}{\xi_1-\xi_2}\right] \tag{1}$$

$$q_A^{IF} = \frac{1}{2\alpha d}\ln\left[\frac{\xi_1+\xi_2}{\xi_2-\xi_1}\right] \tag{2}$$

where $\alpha = \frac{1}{2}\sqrt{\left|\varepsilon_{1t}(\omega)/\varepsilon_{1z}(\omega)\right|}$, $\xi_1 = \sqrt{\left|\varepsilon_{1z}(\omega)\varepsilon_{1t}(\omega)\right|}$, $\xi_2 = \sqrt{\left|\varepsilon_{2z}(\omega)\varepsilon_{2t}(\omega)\right|}$, and d is the quantum well thickness. The GaN quantum well thickness d is set to a default value of 5 nm in the following calculations unless otherwise specified. The phonon wave vectors q_S^{IF} and q_A^{IF} must be real and positive which implies that symmetric and asymmetric modes are distinguished based on the polarity of $\xi_1 - \xi_2$.

The resonant interface phonon frequency is obtained from $\xi_1 = \xi_2$. The $\omega_{TO,res}$ and $\omega_{LO,res}$ are the TO and LO resonant interface frequencies where ξ_1 and ξ_2 are equal in the TO and LO phonon frequency range, respectively. These frequencies are calculated as $\omega_{TO,res}$ = 577.8 cm^{-1} and $\omega_{LO,res}$ = 832.3 cm^{-1}. From the definition of the symmetric and asymmetric phonon wave vectors, the symmetric mode is only defined in the frequency range where $\xi_1 > \xi_2$ and the asymmetric mode is only defined in the range where $\xi_1 < \xi_2$. Combined with the constraints of the dielectric constants, the symmetric TO interface modes can only be defined in the phonon frequency range (ω_{1t}, $\omega_{TO,res}$) and the symmetric LO modes in the range ($\omega_{LO,res}$, ω_{2Lz}). Similarly, the asymmetric TO interface phonons are only defined in ($\omega_{TO,res}$, ω_{2z}) and the asymmetric LO modes in (ω_{1Lt}, $\omega_{LO,res}$).

To investigate the scattering rate between electrons and interface phonons, we adapt the expression from our previous work:

$$\frac{1}{\tau_e^{(a)}} = \pm\frac{2me_0^2}{\hbar^2}\sum_n\int_{\omega_1}^{\omega_2}\frac{\left\{N(\omega)+\frac{1}{2}\mp\frac{1}{2}\right\}D(q,\omega)\sigma\left[\left\{\frac{\omega}{q^2}\pm\frac{\hbar}{2m}\right\}\frac{dq}{d\omega}-\frac{1}{q}\right]}{\left[\frac{q}{2}\pm\frac{m}{\hbar}\left\{\frac{\omega}{q}-\frac{d\omega}{dq}\right\}\right]\sqrt{\frac{1}{m}\chi(\mathbf{k},q,\omega)}}d\omega \tag{7}$$

with

$$\chi(\mathbf{k},q,\omega) = \frac{\hbar^2\mathbf{k}^2}{m}-\frac{\hbar^2q^2}{4m}\pm\hbar\omega-m\frac{d\omega}{dq} \tag{8}$$

$$\sigma = \begin{cases} 0 & \text{for } \chi(\mathbf{k}, q, \omega) < 0 \\ 1 & \text{otherwise} \end{cases} \tag{9}$$

where $m = m^* m_0$, the dimensionless effective mass is $m^* = 0.22$, m_0 is the electron rest mass, e_0 is the elementary charge, and $N(\omega) = \frac{1}{e^{\hbar\omega/k_B T} - 1}$ is the phonon occupation number. The upper (lower) signs are taken when considering electron absorption (emission) scattering process. The summation over n is included to consider scattering with all possible symmetric and asymmetric confined mode phonons. In our numerical calculation of the scattering rates, we find that a practical number for the upper limit is n = 5; contributions from confined modes with n larger than 5 are negligible. For each n (except for the n = 0 case), the symmetric and asymmetric confined modes must be considered separately as the dispersion relations are different from each other. For the case of interface modes, the summation is omitted.

In our original formula, where the integral is assessed over the angle θ between the phonon wave vector q and the optical axis c, the lower and upper limits of the integral are set to $\theta = 0$ and 2π. In order to separately calculate the matrix elements of the Fermi golden rule for each phonon mode of uniaxial wurtzite crystals, the formula with the integral over θ is transformed into an integral over ω. Considering the energy and momentum conservation of the electron–phonon scattering process, the limits of the integral over ω may also be transformed according to the relations:

$$\cos\theta = \begin{cases} \dfrac{m\omega}{kq\hbar} - \dfrac{q}{2k} & \text{for absorption} \\ \dfrac{m\omega}{kq\hbar} + \dfrac{q}{2k} & \text{for emission} \end{cases} \tag{10}$$

Herein, we calculate the scattering rates between the electrons and optical phonons. Fig. 5 shows the (a) interface and (b) confined mode phonon scattering rates as a function of electron energy $E_{\mathbf{k}}$. For both (a) interface and (b) confined modes, the black solid line shows the total scattering rate which combines all contributions from each process indicated as dashed and dotted color lines. The general behavior of the scattering rate curves for both modes are similar. The LO emission scattering rates [(a) red and (b) orange dashed lines] start to dominate once the electron energy exceeds the threshold energy. The TO absorption processes are negligible compared to the others (not plotted in the figures). Due to mode mixing in wurtzites, the TO emission scattering rate is comparable to the LO absorption scattering rate. This causes the total scattering rate to show a two-step-like shape. The total scattering rate of both modes show roughly similar values that converge to ~10^{13} s^{-1} with $E_{\mathbf{k}}$ = 0.3 eV in the current system where the GaN thickness is set to d = 5 nm.

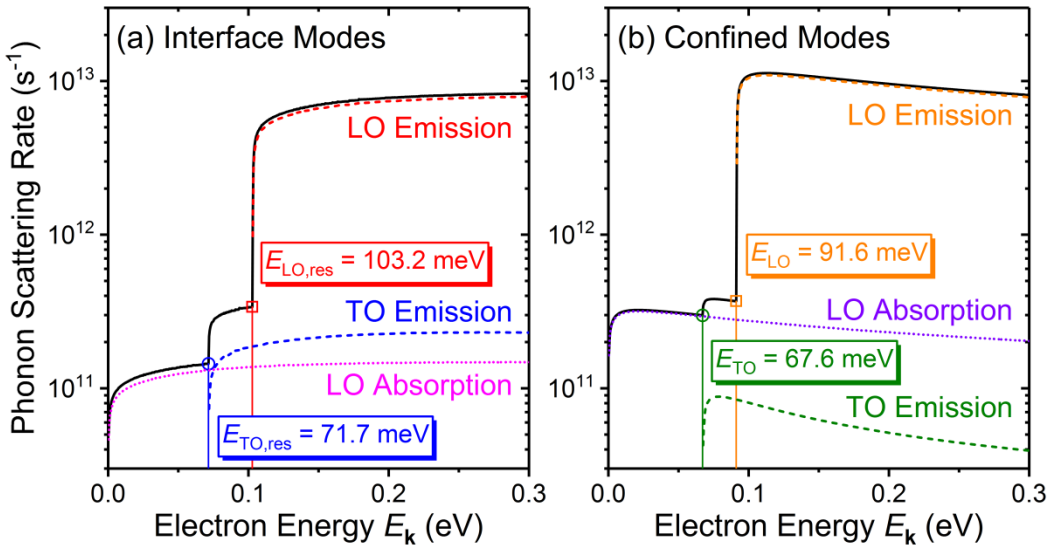

Fig. 5. (a) Interface and (b) confined mode phonon scattering rates are calculated and plotted as a function of electron energy. For both modes, the total interface phonon scattering rate combining all phonon modes (including the TO absorption scattering rate) is shown as the black solid line. The droplines with symbols are shown to indicate the threshold energies of TO emission and LO emission scattering. For interface mode scattering, these energies correspond to the TO and LO interface phonon resonant frequency energies $\hbar\omega_{TO,res}$ = 71.7 meV and $\hbar\omega_{LO,res}$ = 103.2 meV, respectively. For confined mode scattering, the threshold energies are at the vicinity (but not a complete match) of the TO and LO phonon energies of GaN, $\hbar\omega_{1z}$ = 65.8 meV and $\hbar\omega_{1Lt}$ = 91.9 meV, respectively.

Fig. 6. shows the interface and confined mode phonon emission scattering rates of an AlN/GaN/AlN double heterostructure with GaN thickness of d = 1 nm. Compared to the previous d = 5 nm case shown in Fig. 5, indeed, the interface mode scattering rate (red solid line) becomes approximately 8 times larger than the confined mode scattering rate (blue dashed line) for electron energy larger than 0.12 eV. Also notice that the interface mode scattering curve shows more than two of the step-like features. This is due to the emission threshold energy split between the symmetric and asymmetric interface modes. With d = 5, the wave vector q is only large enough to satisfy the emission condition at phonon frequencies of $\omega = \omega_{TO(LO),res}$. However, with smaller d, this is no longer the case and the condition is satisfied with phonon frequencies slightly away from the resonant frequencies. As the symmetric and asymmetric interface modes are defined in separate phonon frequencies, except at the limit of $\omega \rightarrow \omega_{TO(LO),res}$, the threshold energies are split and causes the scattering rate curve to show more step-like increases.

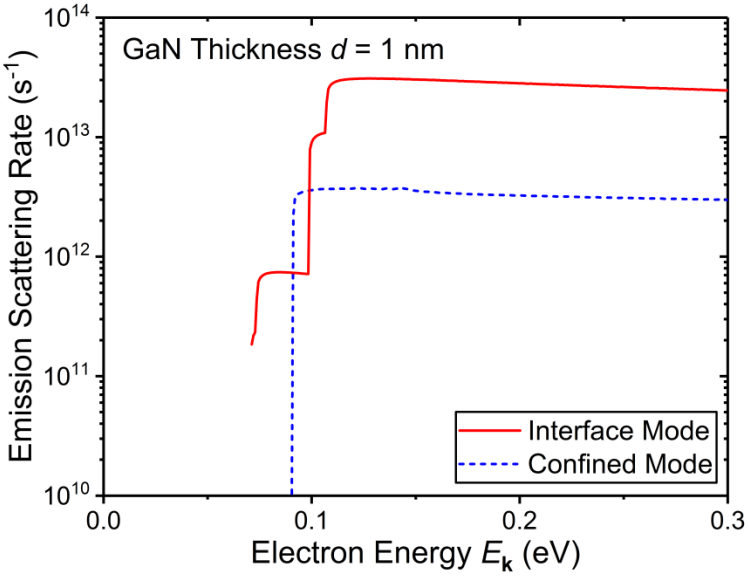

Fig. 6. Interface and confined mode phonon emission scattering rates of a AlN/GaN/AlN double heterostructure with GaN thickness of d = 1 nm is plotted. Compared to the d = 5 nm case, the interface mode scattering rate (red solid line) show a factor of 3 increase, whereas the confined mode scattering rate (blue dashed line) show a factor of 2.5 decrease. Overall, the interface phonon scattering rate is approximately 8 times larger than the confined mode scattering rate with GaN thickness of d = 1 nm.

These results show that III-nitrides can be engineered so that the hot-electron produced LO phonons are produced dominantly in the interface phonon channel; these phonons have high group velocities and the result is that the region where the decaying LO phonons.

During this period we have studied the effect of quantum confinement on the lifetime of anharmonic decay of optical phonons in semiconductor nanostructures. This fundamental phenomenon has not been studied previously for confined structures and it is essential to understand this effect since the production of heat carrying acoustic phonons depends on the lifetime of the parent optical phonons. As is well known, the decay of optical phonons into acoustic phonons is a key step in the production of heat from hot electrons since these hot electrons emit optical phonons. The decay lifetime of LO phonons in bulk GaAs has been evaluated extensively theoretically and experimentally [15-18] unlike the case for nanostructured GaAs. In principle, the cubic anharmonicity of the harmonic oscillator energy the phonon modes lead to phonon decay and interaction with other phonons. Employing regular perturbation theory, Klemens demonstrated decay of zone center longitudinal optical phonons in bulk GaAs where it decays into two longitudinal acoustic phonons with the same energies but opposite momentum [15]. Like Klemens channel, optical phonons in bulk GaAs can also decay in a transverse acoustic phonon and Brillouin zone edge optical phonon according to the experimental work of Valley and Bogani (VB) [18]. However, both processes being N-processes, the crystal momentum and phonon energy remain conserved. Though decay process of the optical phonons has been evaluated theoretically and experimentally to understand various material properties, very few efforts have been directed towards understanding the modification of these processes due to spatial confinement of test device structure.

For last two decades, the effect of dimensional confinement on electron and phonon transport have been comprehensively estimated [19-23]. During this period, the focus of the phonon research community was on anharmonic decay of phonons in bulk structures specifically, only Li et al. [24] evaluated the lifetime of LO phonon in GaAs quantum dots and by Dyson et al. in GaN heterostructures [25]. Only recently researchers have started to investigate the lifetime and dynamics of anharmonic decay of acoustic phonons in other acoustic phonons in confined structures [26,27] to evaluate the heat transport in materials like Si and Ge, important for thermoelectric applications. To the best of our knowledge none of the prior efforts has been directed towards the investigation of the effect of phonon confinement on anharmonic decay of optical phonons in GaAs, which has been considered in this work. The continuum phonon formulation used in this article for GaAs can be extended to isotropic materials with cubic crystal symmetry.

In this article, we have considered the effect of both optical phonon and acoustic phonon confinement on the anharmonic decay rate of the confined optical phonons through Klemens channel and Valle-Bogani channel using the three-phonon interaction Hamiltonian and employed the Fermi golden rule to evaluate the transition probability (TP). The effect of confinement on the TP value has been evaluated in comparison to the bulk case through the calculation of interaction matrix (IM) squared. The first section of the article summarizes the transition probability expression for the bulk case. Thereafter, this paper presents an evaluation of the expression for the relative displacement for a confined optical phonon and the TP has been evaluated for AlAs- and GaAs- based double interface heterostructure quantum well (DHSQW) where acoustic phonons are not confined. The penultimate section, sheds some light on specialized cases where acoustic phonons are also confined in a GaAs free-standing quantum well (FSQW) structure. The average IM squared values in the article are marked as following:

Table 1. Different notation for IM related to different decay process in DHSQW and FSQW

decay process mentioned	**volume average IM notation**
Decay of LO phonon in bulk system (K= Klemen's channel; VB= Vallee-Bogani Channel)	$M_{B,K}, M_{B,VB}$
Klemens type decay in DHSQW	M_C^D

Vallee - Bogani type decay in FSQW (cases 1 and 2 = asymmetric and symmetric CAP*)	$M_C^{F,VB,1}, M_C^{F,VB,2}$
Klemens type decay in FSQW (cases 1, 2, and 3= 2 dilatational type CAP, 2 flexural type CAP, and 1dilatational and 1 flexural type CAP)	$M_C^{F,K,1}, M_C^{F,K,2}, M_C^{F,K,3}$

*CAP: Confined Acoustic phonon

The interaction Hamiltonian within the continuum approximation for three phonon processes can be written as [17]

$$H_3 = \frac{1}{3!\sqrt{N}} P(k, j; k', j'; k'', j'')\, u_{k,j} u_{k',j'} u_{k'',j''} \tag{11}$$

where k, k', k'' are the three phonon wave vectors involved in the annihilation or creation process, j, j', j'' are the polarizations of the three phonons and N is the number of unit cells present. P describes the cubic (anharmonic) coupling and $u_{k,j}$ signifies the displacement field associated with the annihilated or emitted phonons. The phonon displacement in normal coordinates can be represented as:

$$u_{k,j} = \left(\frac{\bar{h}}{2m\omega_{k,j}}\right)^{\frac{1}{2}} e'_{k,j}\left(a_{k,j} e^{i\vec{k}\vec{r}} + a^{\dagger}_{k,j} e^{-i\vec{k}\vec{r}}\right) \tag{12a}$$

$$u(\vec{r}) = \frac{1}{\sqrt{N}} \sum_k \sum_{j=1,2,3} \left(\frac{\bar{h}}{2m\omega_{q,j}}\right)^{\frac{1}{2}} \left(a_{k,j} e^{i\vec{k}\vec{r}} \widehat{e_{k,j}} + a^{\dagger}_{k,j} e^{-i\vec{k}\vec{r}} \widehat{e_{k,j}}^{*}\right) = \frac{1}{\sqrt{N}} \sum_k \sum_{j=1,2,3} \overrightarrow{u_{k,j}} \tag{12b}$$

where $a_{k,j}$, $a^{\dagger}_{k,j}$ denotes the annihilation and creation operator, respectively, $e'_{k,j}$ is the polarization vector, m is the reduced mass of the lattice atoms and $\omega_{k,j}$ is the frequency of the normal mode [25]. Substituting the normalized displacement expression in (1) the three-phonon anharmonic interaction term for type 2 phonon interaction where one phonon decays into two phonons can be written as:

H_3

$$= \frac{1}{V}\int d^3r\ \frac{1}{\sqrt{N}}\left(\frac{\bar{h}}{2m}\right)^{\frac{3}{2}}\left(\frac{1}{\omega_{k,j}\omega_{k',j'}\omega_{k'',j''}}\right)^{\frac{1}{2}} P\ \left(a_{k,j}a^{\dagger}_{k',j'}a^{\dagger}_{k'',j''}\right)\left(\widehat{e_{k,j}}.\widehat{e_{k',j'}}^{*}.\widehat{e_{k'',j''}}^{*}\right)\exp(i(k - k' - k'').r) \quad (13)$$

where V is the volume of the structure under consideration. Assumption of linear dispersion of the acoustic phonons enforces the polarization vectors to vanish if the longitudinal optical phonon decays into two longitudinal acoustic phonons are considered. The TP for any quantum processes can be calculated using Fermi golden rule and given by:

$$\Gamma = \frac{2\pi}{\bar{h}}\ |\langle n_k - 1, n_{k'}, n_{k''}|H_3|n_k, n_{k'} + 1, n_{k''} + 1\rangle|^2\ \delta(\bar{h}(\omega_k - \omega_{k'} - \omega_{k''})) \quad (14)$$

The average value of IM, $|\langle i|V_3|f\rangle|$ for above mentioned type 2 decay (LO->LA+LA) in the (4) can be expressed as:

$$|M_B|^2 = |\langle i|H_3|f\rangle|^2 = \frac{1}{N}\left(\frac{\bar{h}}{2m}\right)^3\left(\frac{1}{\omega_k\omega_{k'}\omega_{k''}}\right)P^2\ n_k(n_{k'} + 1)(n_{k''} + 1)\delta_{k-k'-k'',G} \quad (15)$$

where $n_k = \left(\exp\left(\frac{\bar{h}\omega_k}{k_B T}\right) - 1\right)^{-1}$ is the Bose-Einstein occupation number, G is the reciprocal lattice vector and P is the anharmonic coupling constant given by $P = -\frac{i}{\sqrt{3}}\frac{M}{v}\gamma\omega_k\omega_{k'}\omega_{k''}$ where M = atomic mass, v sound velocity (longitudinal) and γ is the Gruneisen constant [15]. The average value of IM squared $|M|^2$ for the phonon interaction mentioned in (5) contains the delta function due to the integration of the Hamiltonian in the whole volume as:

$$\frac{1}{V}\int d^3r \exp(i.(k - k' - k'').r) = \delta_{k-k'-k''} \quad (16)$$

Eq. 15 can be further simplified under the assumption that $\omega_k = k * c_k$, i.e. linear dispersion of acoustic waves elaborately discussed in Ref. 28. The average value arises from integration of the exponential term within the whole volume which produces the δ function with a subscript denoting whether the process is an N-process or U-process, determined by G value. Using this isotropic formulation, Klemens et al. [15], Bhatt et al. [17], Srivastava et al. [16] have theoretically calculated the anharmonic lifetime of LO phonons in bulk GaAs slabs to be of 3.5 ps [15-17] at room temperature which has been experimentally verified with 2.2 ± 0.2 ps value [29] using Raman spectroscopy.

The effect of phonon confinement on anharmonic phonon decay is evaluated in two different nanostructure assemblies. The AlAs/GaAs/AlAs DHSQW is the first test structure considered where optical phonon modes in GaAs are confined due to difference in dielectric property between the two materials but acoustic phonons behave as continuum elastic modes as the two materials have almost similar elastic properties. Whereas in second test structure of GaAs FSQW, the acoustic modes are confined because acoustic modes only lie within the QW structure and the stress field is zero at the boundary/interface. The anharmonic coupling constant depends on three main scattering processes [28], a lattice wave can undergo scattering from a point imperfection, single dislocation and grain boundaries. Due to dimensional confinement surface effects become prominent, external boundary scattering of phonons increases but as for anharmonic decay of confined phonons we have assumed that the anharmonic coupling coefficient does not change compared to bulk case. A similar assumption has also been employed in Ref. 33 for the case of a quantum dot.

The confinement of optical phonon arises in both DHSQW and FSQW as the constituent materials have dissimilar dielectric function which in turn depends on the zone center optical phonon frequency. Consideration of previously-mentioned heterostructure with dissimilar dielectric properties produces two main types of phonon modes, namely: a) confined modes (bounded within the well structure) hence the phonon potential should go to zero at the two interfaces, b) Interface mode (localized along the interface) i.e. the potential follows a decaying profile inside the well. Under the dielectric continuum (DC) model assumption, both modes are necessary to represent the optical modes within the structure. Following the DC model, the potential term for optical-phonon modes in a confined polar material structure can be written as:

$$\varphi(q_{II}, z) = \sqrt{\frac{2}{Ad_z}} \begin{Bmatrix} \cos(k_z z) \\ \sin(k_z z) \end{Bmatrix} \exp(\pm i k_{II} \rho) \tag{17}$$

where $k_z = n\pi/d_z$; d_z is the thickness of the quantum well, A = Area of the quantum well and q_{II} is the wavevector parallel to the interfacial plane. The $\cos(q_z z)$ term is obtained when n = odd and for n= even, the displacement function assumes the $\sin(q_z z)$ form in order to force the potential to zero at the interface. As the material is assumed to be isotropic, the displacement pattern of the mode can also be written using Born-Huang theory [16] as:

$$\mathbf{u} = \sqrt{\frac{V}{4\pi\mu N}} \frac{\sqrt{\varepsilon^0 - \varepsilon^\infty}}{\sqrt{\omega_{TO}^2 - \omega^2}} \omega_{TO} \mathbf{E} \quad \text{and} \quad \mathbf{E} = -\boldsymbol{\nabla}\varphi \tag{18}$$

Using Eqs. 17 and 18 the displacement field for confined mode with normal coordinate is given as:

$$u_{k,j} = \left(\frac{\bar{h}}{2m\omega_{k,j}}\right)^{\frac{1}{2}} \left(a_{k,j} \begin{Bmatrix} \cos(k_z z) \\ \sin(k_z z) \end{Bmatrix} \exp(i k_{II} \rho) \widehat{e_{q,j}} + a_{k,j}^{\dagger} \begin{Bmatrix} \cos(k_z z) \\ \sin(k_z z) \end{Bmatrix} \exp(-i k_{II} \rho) \widehat{e_{q,j}}^{*} \right) \tag{19}$$

The value of the constant for displacement is calculated using proper quantization condition given by $\int u(k_{II}, z) * u^*(k_{II}, z) d^3 r = \frac{\bar{h}}{2m\omega}$, where m is based on the mass of the ions in the primitive cell.

Hard confinement of the acoustic modes inside a slab occurs in presence of acoustically mismatched interfaces only. A huge difference is elastic constant causes extreme confinement of acoustic modes, whereas materials with almost similar elastic constant like GaAs and AlAs the interfaces behave as a continuous media hence confinement of acoustic modes is not obtained in this specific structure. Hence, the DHSQW structure behaves as a continuous media for acoustic modes and the mode displacements retain the bulk-type expression form given in Eq. (12).

Unlike DHSQW structure discussed in the previous section, FSQW contains confined acoustic phonons rather than continuum acoustic phonons due to acoustic property difference at the interface. Due to 'hard' confinement effect, the dispersion curves for the acoustic phonons also changes from that of bulk modes. The localized acoustic modes in the slab for an isotropic material using elastic continuum theory and appropriate boundary condition are of three main types: Shear Mode, Dilatational Mode (Symmetric) and Flexural Mode (Anti-Symmetric) [32] which has also been efficiently summarized by Stroscio and Dutta [31]. The mode shape for dilatational, flexural modes and shear modes inside the slab is described in the Table II. The decaying mode shape or interface modes in the embedding material is not described because we are only considering the decay dynamics inside the quantum well region.

Table 2. Displacement function of three types of confined acoustic modes

Mode Type	Displacement envelope inside the slab	
Shear (S)	$u_{S,y}(z) = \begin{cases} \cos(k_{z,n}z), & n = 0,2,4,.. \\ \sin(k_{z,n}z), & n = 1,3,5,... \end{cases}$	(20)
Dilatational/ Symmetric (D)	$u_{D,x}(z) = ik_{II}\left[(k_{II}^2 - k_t^2)\sin\left(\frac{k_t d_z}{2}\right)\cos(k_l z) + 2k_l k_t \cos(k_t z)\sin\left(\frac{k_t d_z}{2}\right)\right]$ $u_{D,z}(z) = k_l\left[-(k_{II}^2 - k_t^2)\sin(\frac{k_t d_z}{2})\sin(k_l z) + 2k_{II}^2 \sin(k_t z)\sin\left(\frac{k_t d_z}{2}\right)\right]$	
Flexural/Anti-Symmetric(F)	$u_{F,x}(z) = ik_{II}\left[(k_{II}^2 - k_t^2)\cos\left(\frac{k_t d_z}{2}\right)\sin(k_l z) + 2k_l k_t \sin(k_t z)\cos\left(\frac{k_t d_z}{2}\right)\right]$ $u_{F,z}(z) = k_l\left[(k_{II}^2 - k_t^2)\cos\left(\frac{k_t d_z}{2}\right)\cos(k_l z) - 2k_{II}^2 \cos(k_t z)\cos\left(\frac{k_t d_z}{2}\right)\right]$	

where $k_{l,n} = ({k_\parallel}^2 - \frac{{\omega_n}^2}{c_l^2})^{1/2}$ and $k_{t,n} = ({k_\parallel}^2 - \frac{{\omega_n}^2}{c_t^2})^{1/2}$ with c_l and c_t are the longitudinal and transverse sound velocity in the isotropic slab medium. The confined acoustic mode displacements are eigenfunctions solution to a eigen-value equation, hence the modes are needed to be orthogonalized for an eigen frequency. The orthogonalized mode displacements for Shear, Dilatational and Flexural modes are given by, $w_{n,S} = F_S u_{S,y}$, $w_{n,D} = F_D(u_{D,x}\hat{x} + u_{D,z}\hat{z})$, and $w_{n,F} = F_S(u_{F,x}\hat{x} + u_{F,z}\hat{z})$ respectively. The normalized mode displacements follow the condition given by $\int w_{n,i}^* w_{m,i} = \delta_{mn}$. Using the normalized modes, the quantized shear, dilatational and flexural modes can be represented as $\sqrt{\frac{\bar{h}}{2m\omega_n}}(a_k + a_k^\dagger) * F_S * (u_{S,y}\hat{\mathbf{y}})\exp(ik_{II}\rho)$, $\sqrt{\frac{\bar{h}}{2m\omega_n}}(a_k + a_k^\dagger) * F_D * (u_{D,x}\hat{\mathbf{x}} + u_{D,z}\hat{\mathbf{z}})\exp(ik_{II}\rho)$ and $\sqrt{\frac{\bar{h}}{2m\omega_n}}(a_k + a_k^\dagger) * F_f * (u_{F,x}\hat{\mathbf{x}} + u_{F,z}\hat{\mathbf{z}})\exp(ik_{II}\rho)$ respectively, three orthonormal modes [33] obtained using Gram Schmidt orthogonalization and second quantization. The normalization constants F_S, F_D and F_f are given in the appendix section and these constants are only dependent on in-plane, wavevector, frequency of the phonon mode, longitudinal or transverse sound velocity and thickness of the well. The x-component of Flexural mode and Dilatational mode was found to be symmetric and asymmetric respectively; similarly, for z component the modes are found to be asymmetric and symmetric respectively. Due to quantum confinement in the z direction the acoustic wavevector along z-direction will be quantized i.e. for all value of k_{II} there will be only few $k_{l,n}$ and $k_{t,n}$ possible which are given by the dispersion curves. The $k_{l,n}$ is imaginary and $k_{t,n}$ is real for fundamental dilatational mode and both are imaginary for fundamental flexural mode for low $k_\parallel$ value [31]. For a FSQW structure, the confined mode pattern will also depend on the boundary condition (BC) as free boundary condition

will force the stress at the interfaces to be zero. Whereas the clamped boundary condition (GaAs is embedded in a very dissimilar material) will enforce that the displacement at interface goes to zero.

In DHSQW structures, the confinement is only in the z-direction and in the x-y direction wave properties behave as bulk or unconfined. Hence, assuming type-2 phonon interaction the Hamiltonian for three phonon interactions can be written as:

$$H_3' = \frac{1}{A}\int \frac{d\rho}{\sqrt{N}}\left(\frac{\bar{h}}{2m}\right)^{\frac{3}{2}}\left(\frac{1}{\omega_{k,j}\omega_{k',j'}\omega_{k'',j''}}\right)^{\frac{1}{2}} P\left(a_{k,j}a^{\dagger}_{k',j'}a^{\dagger}_{k'',j''}\right)\left(\widehat{e_{k,j}}.\widehat{e_{k',j'}}^{*}.\widehat{e_{k'',j''}}^{*}\right)$$
$$\begin{Bmatrix}\cos(k_z z)\\ \sin(k_z z)\end{Bmatrix}\exp(-i(k_z' + k_z'')z)\exp(i(k_{II} - k_{II}' - k_{II}'').\rho) \quad (21)$$

where $\mathbf{k^a} = k_z^a\hat{\mathbf{z}} + k_{II}^a\hat{\boldsymbol{\rho}}$**.** Using similar arguments as mentioned for the bulk case, the interaction Hamiltonian is obtained after integrating the last term in the expression as:

$$H_3' = \frac{1}{\sqrt{N}}\left(\frac{\bar{h}}{2m}\right)^{\frac{3}{2}}\left(\frac{1}{\omega_{k,j}\omega_{k',j'}\omega_{k'',j''}}\right)^{\frac{1}{2}} P\left(a_{k,j}a^{\dagger}_{k',j'}a^{\dagger}_{k'',j''}\right)\left(\widehat{e_{k,j}}.\widehat{e_{k',j'}}^{*}.\widehat{e_{k'',j''}}^{*}\right)$$
$$\begin{Bmatrix}\cos(k_z z)\\ \sin(k_z z)\end{Bmatrix}\exp(-i(k_z' + k_z'')z)\delta_{k_{II}-k_{II}'-k_{II}'',G_{II}} \quad (22)$$

The previously mentioned three phonon interaction suggests that the in-plane vector should be conserved to produce δ_{00} and for all other combination the interaction Hamiltonian is zero. The IM squared value for calculating TP for the confined optical phonons can be obtained using Fermi golden rule similar to the bulk case and the average value of that IM squared due to confinement over d_z along z-direction is given by:

$$\left|M_C^D\right|^2 = |\langle n_k - 1, n_{k'}, n_{k''}|H_3|n_k, n_{k'} + 1, n_{k''} + 1\rangle|^2$$
$$= \frac{1}{d_z}\int_{-d_z/2}^{d_z/2} dz \frac{1}{N}\left(\frac{\bar{h}}{2m}\right)^3\left(\frac{1}{\omega_k\omega_{k'}\omega_{k''}}\right)P^2\begin{Bmatrix}\cos^2(k_z z)\\ \sin^2(k_z z)\end{Bmatrix} n_k(n_{k'} + 1)(n_{k''} + 1)$$
$$\exp(-i(k_z' + k_z'')z)\delta_{k_{II}-k_{II}'-k_{II}'',G_{II}}$$
$$\therefore \left|M_C^D\right|^2 = \frac{1}{N}\left(\frac{\bar{h}}{2m}\right)^3\left(\frac{1}{\omega_k\omega_{k'}\omega_{k''}}\right)P^2 n_k(n_{k'} + 1)(n_{k''} + 1)\delta_{k_{II}-k_{II}'-k_{II}'',G_{II}}$$
$$\int_{-d_z/2}^{d_z/2}\begin{Bmatrix}\cos^2(k_z z)\\ \sin^2(k_z z)\end{Bmatrix}\exp(-2i(k_z' + k_z'')z)dz \quad (23)$$

Based on the Fuchs-Kliewer slab mode boundary condition, the z-component of the displacement can only take the form of $\sin(k_z z)$. Evaluation of the integral produces (for $k_z' = -k_z''$):

$$\frac{1}{d_z}\int_{-d_z/2}^{d_z/2} sin^2\left(\frac{\pi}{d_z}z\right)dz = \frac{1}{2} \quad (24a)$$

and for

$$k_z' \neq -k_z''$$

$$\frac{1}{d_z}\int_{\frac{-d_z}{2}}^{\frac{d_z}{2}} sin^2(k_z z)\, exp(-2i(k_z' + k_z'')z)\, dz = \frac{(2(k_z' + k_z'')^2 d_z^2 - \pi^2)\, sin\big((k_z' + k_z'')d_z\big)}{d_z\big(2(k_z' + k_z'')^3 d_z^2 - 2\pi^2(k_z' + k_z'')\big)} \tag{24b}$$

In GaAs, the zone center LO phonon decays into two LA phonons of same phonon polarization with opposite momentum through the Klemens channel. According to momentum conservation, the in-plane wavevector of two daughter acoustic waves are related through $k_{II}' = -k_{II}''$ if the parent optical phonon is zone center; whereas k_z' and k_z'' will be equal and opposite if the two acoustic modes are in $\Gamma - L$ direction. Otherwise if daughter phonons are along $\Gamma - K$ symmetry direction $k_z' = k_z'' = 0$. Hence, for decay of zone center LO phonon in GaAs, the integral is reduced to (24a). But for any other decay processes, if the acoustic phonons are not on the same polarization branch then the k_z' and k_z'' can be evaluated from $\left(\left(\frac{\omega_{k'}}{c_{l,t}}\right)^2 - {k_{II}'}^2\right)^{\frac{1}{2}}$ and $\left(\left(\frac{\omega_{k''}}{c_{l,t}}\right)^2 - {k_{II}''}^2\right)^{\frac{1}{2}}$ where $\omega_{k'}$ and $\omega_{k''}$ are the acoustic phonon frequency and $c_{l,t}$ is the sound speed along the direction (for longitudinal phonon) or perpendicular to the acoustic phonon wavevector. Combining Eq. (23) with (14a) the IM squared can be written as:

$$\left|M_C^D\right|^2 = \frac{1}{N}\left(\frac{\bar{h}}{2m}\right)^3 \left(\frac{1}{\omega_k \omega_{k'} \omega_{k''}}\right) P^2 n_k (n_{k'} + 1)(n_{k''} + 1)\delta_{k_{II} - k_{II}' - k_{II}'', G_{II}} \cdot \frac{1}{2}$$
$$\therefore \left|M_C^D\right|^2 = \left|M_{B,K}\right|^2 \cdot \frac{1}{2} \tag{25}$$

where $\left|M_{B,K}\right|^2$ is the IM squared value bulk material for Klemens channel. Hence for the decay rate of Klemens channel in a confined structure with respect to a bulk case in GaAs can be written as:

$$\Gamma(\text{confined}) = \frac{1}{\tau(\text{confined})} = \frac{1}{2}\Gamma(\text{bulk}) = \frac{1}{2\tau(\text{bulk})} \tag{26}$$

Employing the mathematical description of optical phonon given in section II-A and description of acoustic phonon in II-D, the three-phonon interaction Hamiltonian can be obtained analogous to the DHSQW structure. Following Eq. 22 the average IM squared can be written as:

$$\left|M_C^F\right|^2 = \frac{1}{N}\left(\frac{\bar{h}}{2m}\right)^3 \left(\frac{1}{\omega_k \omega_{k'} \omega_{k''}}\right) P^2 n_k (n_{k'} + 1)(n_{k''} + 1)\delta_{k_{II} - k_{II}' - k_{II}'', G_{II}} \frac{1}{d_z}\int_{-d_z/2}^{d_z/2} v(z)dz \tag{27}$$

where $v(z)$ can be determined by considering the expression for optical and acoustic phonon given in (9) and (17) and the decay process of interest. The frequency, wavevector and polarization of the three phonons involved in the process are determined by considering the energy conservation principle, crystal momentum conservation and symmetry plane of interaction. The two daughter acoustic phonons for Klemen's channel decay can be two dilatational or two flexural or one dilatational and one flexural modes and as shear modes represents purely transverse vibrations it will only be participating in Vallee-Bogani (VB) channel evaluation where a zone-edge LO and a

TA phonon are created. For different decay processes the v(z) differs due to the complicated mode pattern of the confined acoustic modes.

The shear mode represents pure transverse modes and the mode pattern appears to be of the form $\cos(k_{z,n}z)$ or $\sin(k_{z,n}z)$. The two optical phonon mode patterns for the VB channel will follow the sin function in order to satisfy the boundary condition on phonon potential. Employing the optical phonon mode pattern given in Eq. 19 and sinusoidal shear acoustic wave mode pattern, the v(z) is given by:

$$v(z) = F_1(z) = \sin^6\left(\frac{\pi z}{d_z}\right) \tag{28a}$$

$$v(z) = F_2(z) = \cos^2\left(\frac{\pi z}{d_z}\right)\sin^4\left(\frac{\pi z}{d_z}\right) \tag{28b}$$

where $F_1(z)$ denoted the case where both LO and TA phonon are of $\sin(k_{z,n}z)$ form and $F_2(z)$ represents the shear TA mode is in $\cos(k_{z,n}z)$ form and LO mode is in $\sin(k_{z,n}z)$ form. The corresponding IM squared for $F_1(z)$ and $F_2(z)$ are obtained as following:

$$\left|M_C^{F,VB,1}\right|^2 = \frac{1}{Nd_z}\left(\frac{\bar{h}}{2m}\right)^3\left(\frac{F_s^4}{\omega_k\omega_{k'}\omega_{k''}}\right)P^2 n_k(n_{k'}+1)(n_{k''} + 1)\delta_{k_{II}-k'_{II}-k''_{II},G_{II}}\int_{\frac{-d_z}{2}}^{\frac{d_z}{2}} F_1(z)dz$$

$$\left|M_C^{F,VB,1}\right|^2 = \frac{5}{16}\frac{1}{N}\left(\frac{\bar{h}}{2m}\right)^3\left(\frac{F_s^4}{\omega_k\omega_{k'}\omega_{k''}}\right)P^2 n_k(n_{k'}+1)(n_{k''}+1)\delta_{k_{II}-k'_{II}-k''_{II},G_{II}}$$

$$\therefore \left|M_C^{F,VB,1}\right|^2 = \frac{5}{16}F_s^4\left|M_{B,VB}\right|^2 \tag{29a}$$

$$\left|M_C^{F,VB,2}\right|^2 = \frac{1}{Nd_z}\left(\frac{\bar{h}}{2m}\right)^3\left(\frac{F_s^4}{\omega_k\omega_{k'}\omega_{k''}}\right)P^2 n_k(n_{k'}+1)(n_{k''} + 1)\delta_{k_{II}-k'-k'',G_{II}}\int_{-d_z/2}^{d_z/2} F_2(z)dz$$

$$\left|M_C^{F,VB,2}\right|^2 = \frac{1}{16}\frac{1}{N}\left(\frac{\bar{h}}{2m}\right)^3\left(\frac{F_s^4}{\omega_k\omega_{k'}\omega_{k''}}\right)P^2 n_k(n_{k'}+1)(n_{k''}+1)\delta_{k_{II}-k'_{II}-k''_{II},G_{II}}$$

$$\therefore \left|M_C^{F,VB,2}\right|^2 = \frac{1}{16}F_s^4\left|M_{B,VB}\right|^2 \tag{29b}$$

$M_{B,VB}$ is the IM squared value for Vallee-Bogani channel in bulk GaAs material.

As for Klemens type of decay the two daughter LA phonons can be of a combination of dilatational and flexural mode pattern, as mentioned earlier. For all three cases the optical and acoustic vibrations lie in the x-z plane assuming z is perpendicular to the interfaces. As the two modes comprise of complimentary variations along both x and z axis, we considered only x-direction displacement in order to simplify the problem. We have assumed the magnitude of x-displacement in a simpler form given as:

$$u_{D,x} = A_1\cos(k_l z) + B_1\cos(k_t z)$$

(Symmetric)
Flexural

$$u_{F,x} = A_2 \sin(k_l z) + B_2 \sin(k_t z) \tag{30}$$

(Asymmetric)

where $A_1 = F_D k_{II}(k_{II}^2 - k_t^2) \sin\left(\frac{k_t d_z}{2}\right)$, $A_2 = F_f k_{II}(k_{II}^2 - k_t^2) \cos\left(\frac{k_t d_z}{2}\right)$, $B_1 = F_D 2k_{II}k_l k_t \sin\left(\frac{k_t d_z}{2}\right)$ and $B_2 = F_f 2k_{II}k_l k_t \cos\left(\frac{k_t d_z}{2}\right)$. Assuming the co-linearity of three phonons displacement, the $v(z)$ function for three cases are calculated using fundamental wavevector value and the IM squared for those cases. The k_l and k_t value are assumed to be real for all three cases to ensure the existence of the confined modes inside the quantum well, imaginary value of the wavevector forces the modes to be only surface bound.

Table 3. The evaluation of the $v(z)$ function for three different acoustic modes

Both D mode	$v(z) = F_3(z) = \sin^2\left(\frac{\pi z}{d_z}\right)\left(A_1 \cos\left(\frac{\pi}{d_z} z\right) + B_1 \cos\left(\frac{\pi}{d_z} z\right)\right)^4$
	$\frac{1}{d_z}\int_{-d_z/2}^{d_z/2} F_3(z)dz = \frac{1}{16}(A_1 + B_1)^4$
Both F mode	$v(z) = F_4(z) = \sin^2\left(\frac{\pi z}{d_z}\right)\left(A_2 \sin\left(\frac{\pi}{d_z} z\right) + B_2 \sin\left(\frac{\pi}{d_z} z\right)\right)^4$
	$\frac{1}{d_z}\int_{-d_z/2}^{d_z/2} F_4(z)dz = \frac{5}{16}(A_2 + B_2)^4$
(1D+1F) mode	$v(z) = F_5(z) = \sin^2\left(\frac{\pi z}{d_z}\right)\left(A_1 \cos\left(\frac{\pi}{d_z} z\right) + B_1 \cos\left(\frac{\pi}{d_z} z\right)\right)^2 \left(A_2 \sin\left(\frac{\pi}{d_z} z\right) + B_2 \sin\left(\frac{\pi}{d_z} z\right)\right)^2$
	$\frac{1}{d_z}\int_{-d_z/2}^{d_z/2} F_5(z)dz = \frac{1}{16}(A_1 + B_1)^2(A_2 + B_2)^2$

Replacing the three functions obtained in Table-III in (27) the IM squared for the three processes are given as:

$$\left|M_C^{F,K,1}\right|^2 = \frac{1}{16}(A_1 + B_1)^4 \frac{1}{N}\left(\frac{\bar{h}}{2m}\right)^3 \left(\frac{1}{\omega_k \omega_{k'} \omega_{k''}}\right) P^2 n_k (n_{k'} + 1)(n_{k''} + 1)\delta_{k_{II} - k'_{II} - k''_{II}, G_{II}} \tag{31a}$$

$$\therefore \left|M_C^{F,K,1}\right|^2 = \frac{1}{16}(A_1 + B_1)^4 \left|M_{B,K}\right|^2$$

$$\left|M_C^{F,K,2}\right|^2 = \frac{5}{16}(A_2 + B_2)^4 \frac{1}{N}\left(\frac{\bar{h}}{2m}\right)^3 \left(\frac{1}{\omega_k \omega_{k'} \omega_{k''}}\right) P^2 n_k (n_{k'} + 1)(n_{k''} + 1)\delta_{k_{II} - k'_{II} - k''_{II}, G_{II}} \tag{31b}$$

$$\therefore \left|M_C^{F,K,2}\right|^2 = \frac{5}{16}(A_2 + B_2)^4 \left|M_{B,K}\right|^2$$

$$\left|M_C^{F,K,3}\right|^2 = \frac{1}{16}(A_1 + B_1)^2(A_2 + B_2)^2 \frac{1}{N}\left(\frac{\bar{h}}{2m}\right)^3 \left(\frac{1}{\omega_k \omega_{k'} \omega_{k''}}\right) P^2 n_k (n_{k'} + 1)(n_{k''} + 1)\delta_{k_{II} - k'_{II} - k''_{II}, G_{II}}$$

$$\therefore \left|M_C^{F,K,3}\right|^2 = \frac{1}{16}(A_1 + B_1)^2(A_2 + B_2)^2 \left|M_{B,K}\right|^2 \quad (31c)$$

where $M_{B,K}$ is the IM squared value bulk material for Klemens channel. Using all the IM matrix squared value the transition probability or inverse of lifetime can be calculated. The bulk IM squared value for all above mentioned decay processes are decay process specific, hence calculation of the decay lifetime for confined structures requires knowledge of the decay for bulk case. Using Fermi golden rule, the transition probabilities are calculated as:

$$\begin{aligned}
\Gamma_{B,VB/K} &= \frac{2\pi}{\bar{h}} \left|M_{B,VB/K}\right|^2 \delta(\bar{h}(\omega_k - \omega_{k'} - \omega_{k''})) \\
\Gamma_{C,K}^{D} &= \frac{2\pi}{\bar{h}} \left|M_C^{D}\right|^2 \delta(\bar{h}(\omega_{k,n} - \omega_{k'} - \omega_{k''})) \\
\Gamma_{C,VB}^{F,1} &= \frac{2\pi}{\bar{h}} \left|M_C^{F,VB,1}\right|^2 \delta(\bar{h}(\omega_{k,n} - \omega_{k',n} - \omega_{k'',n})) \\
\Gamma_{C,K}^{F,1} &= \frac{2\pi}{\bar{h}} \left|M_C^{F,K,1}\right|^2 \delta(\bar{h}(\omega_{k,n} - \omega_{k',n} - \omega_{k'',n}))
\end{aligned} \quad (32)$$

where $\Gamma_{c,b}^{a,d}$ denotes the transition probability of the process under confinement and a can be {F=FSQW, D=DHSQW}, d can have values {1,2,3; depending on whether the CAPs are asymmetric or asymmetric}, c denoted {C= confined, B= Bulk} and b is the {VB, K; type of decay process}. The difference between $\omega_i, \omega_{i,n}$ is that first term denotes frequency of the phonons in bulk and the later in confined structure.

In the previous discussion, the quantization constant for shear, dilatational and flexural acoustic modes are given in the following section. The constants are obtained using the second quantization where acoustic mode energies are equal to single phonon energy. As we are only interested in confined modes in this problem we the constants are given for real values of k_l, k_t.
Shear Mode:

$$F_S = \begin{cases} \frac{1}{\sqrt{d_z}}, n = 0 \\ \sqrt{\frac{2}{d_z}}, n > 0 \end{cases} \quad (33)$$

Dilatational mode:

$$\begin{aligned}
F_d^{-2} = \frac{1}{8k_l k_t}\big[&2d_z k_l^3 k_t^5 + 4d_z k_l^3 k_t^3 k_x^2 + 2d_z k_l k_t^5 k_x^2 + 10 d_z k_l^3 k_t k_x^4 + 4 d_z k_l k_t^3 k_x^4 + \\
&2d_z k_l k_t k_x^6 - 8 d_z k_l^3 k_t k_x^2 (k_x^2 + k_t^2)\cos(d_z k_l) - 2 d_z k_l k_t (k_t^2 - k_x^2)(k_l^2 + \\
&k_x^2)\cos(d_z k_t) + 2 k_t (k_x^2 - k_t^2)(k_l^2 k_t^2 + 7 k_l^2 k_x^2 - k_t^2 k_x^2 + k_x^4)\sin(d_z k_l) + \\
&8 k_l^3 k_x^2 (k_t^2 - k_x^2)\sin(d_z k_l) + (k_l^2 k_t^5 + 4 k_l^3 k_t^2 k_x^2 + 6 k_l^2 k_t^3 k_x^2 - k_t^5 k_x^2 - 4 k_l^3 k_x^4 - \\
&7 k_l^2 k_t k_x^4 + 2 k_t^3 k_x^4 - k_t k_x^6)\sin\big(d_z(k_l - k_t)\big) + \big(k_l^2 k_t^5 - 4 k_l^3 k_t^2 k_x^2 + 6 k_l^2 k_t^3 k_x^2 -
\end{aligned} \quad (34)$$

$k_l^5 k_x^2 - 4k_l^3 k_x^4 - 7k_l^2 k_t k_x^4 + 2k_t^3 k_x^4 - k_t k_x^6) \sin(d_z(k_l + k_t))]$

Flexural mode:

$$F_f^{-2} = \frac{1}{8k_l k_t}[2d_z k_l^3 k_t^5 + 4d_z k_l^3 k_t^3 k_x^2 + 2d_z k_l k_t^5 k_x^2 + 10d_z k_l^3 k_t k_x^4 - 4d_z k_l k_t^3 k_x^4 + 2d_z k_l k_t k_x^6 + 8d_z k_l^3 k_t k_x^2 (k_x^2 + k_t^2)\cos(d_z k_l) + 2d_z k_l k_t (k_t^2 - k_x^2)(k_l^2 + k_x^2)\cos(d_z k_t) - 2k_t (k_x^2 - k_t^2)(k_l^2 k_t^2 + 7k_l^2 k_x^2 - k_t^2 k_x^2 + k_x^4)\sin(d_z k_l) + 8k_l^3 k_x^2 (k_x^2 - k_l^2)\sin(d_z k_l) + (k_l^2 k_t^5 + 4k_l^3 k_t^2 k_x^2 + 6k_l^2 k_t^3 k_x^2 - k_t^5 k_x^2 - 4k_l^3 k_x^4 - 7k_l^2 k_t k_x^4 + 2k_t^3 k_x^4 - k_t k_x^6)\sin(d_z(k_l - k_t)) + (k_l^2 k_t^5 - 4k_l^3 k_t^2 k_x^2 + 6k_l^2 k_t^3 k_x^2 - k_l^5 k_x^2 - 4k_l^3 k_x^4 - 7k_l^2 k_t k_x^4 + 2k_t^3 k_x^4 - k_t k_x^6)\sin(d_z(k_l + k_t))] \quad (35)$$

where k_x denotes the in-plane wavevector which is equivalently noted here as k_{II} for both flexural and dilatational modes.

lowest values for k_x, k_l and k_t are limited by the device dimensions in the in-plane direction and dimension in confined direction. The lowest values for k_t and k_t are 3.14×10^8 for a $10\ nm$ thick quantum well. For a 10 nm thick quantum well:

$$F_S = \sqrt{\frac{2}{10^{-8}}} = 14142\ m^{-1/2}$$

$$F_d^{-2}, F_f^{-2} \sim \frac{d_z k_t^8}{k_t k_l} \approx 10^{40}$$

$$\therefore\ F_D, F_S \sim 10^{-20}$$

The value for F_D and F_f are calculated approximately and obtained as very small values.

In this research, the effect of dimensional confinement on the anharmonic decay of a longitudinal optical phonon in isotropic cubic crystal (GaAs) is analyzed. The main decay processes considered for GaAs are the Klemens channel (LO -> LA+LA) and the Valle-Bogani Channel (LO -> LO+TA). The confined optical phonons and acoustic phonons are treated using the dielectric continuum model and the elastic continuum model, thereafter the modes are second quantized. The transition probability of the decay process is calculated for a DHSQW, where acoustic phonon modes are continuous, whereas optical phonon modes are confined and FSQW structure where both acoustic and optical phonon modes are confined. The analysis is based on the three-phonon interaction Hamiltonian the interaction matrix squared for both Klemens and Vallee-Bogani decay processes is calculated for DHSQW and FSQW. The calculations suggest that decay probability of Klemens channel reduces by half compared to bulk case for DHSQW and for FSQW the rate is significantly depends on daughter phonons wavevector through non-linear relationship. The decay rate for the processes also depends on the mode pattern, i.e., whether the daughter acoustic phonon modes are symmetric or not. This formulation can be extended to calculate anharmonic decay rate of phonons which have ubiquitous effect on carrier and thermal transport and electron relaxation dynamics in the future nanostructured devices.

Recently, we have made significant progress on generalizing the techniques for determining the infrared active phonon modes in layers III-nitride materials. These results allow us to determine the infrared active phonon frequencies and Frohlich interaction potentials which are essential for modeling carrier transport and phonon emission probabilities underlying the electronic properties of novel manmade III-nitride heterostructures. The case of a GaN/$In_{0.15}Ga_{0.85}$N/GaN heterostructure has also been modeled in this research [34].

Raman spectral analyses have been used to detect the presence of phonon signatures from AlN-GaN superlattices as well as from the sapphire substrate present on many samples. Such a spectrum is in Figure 7.

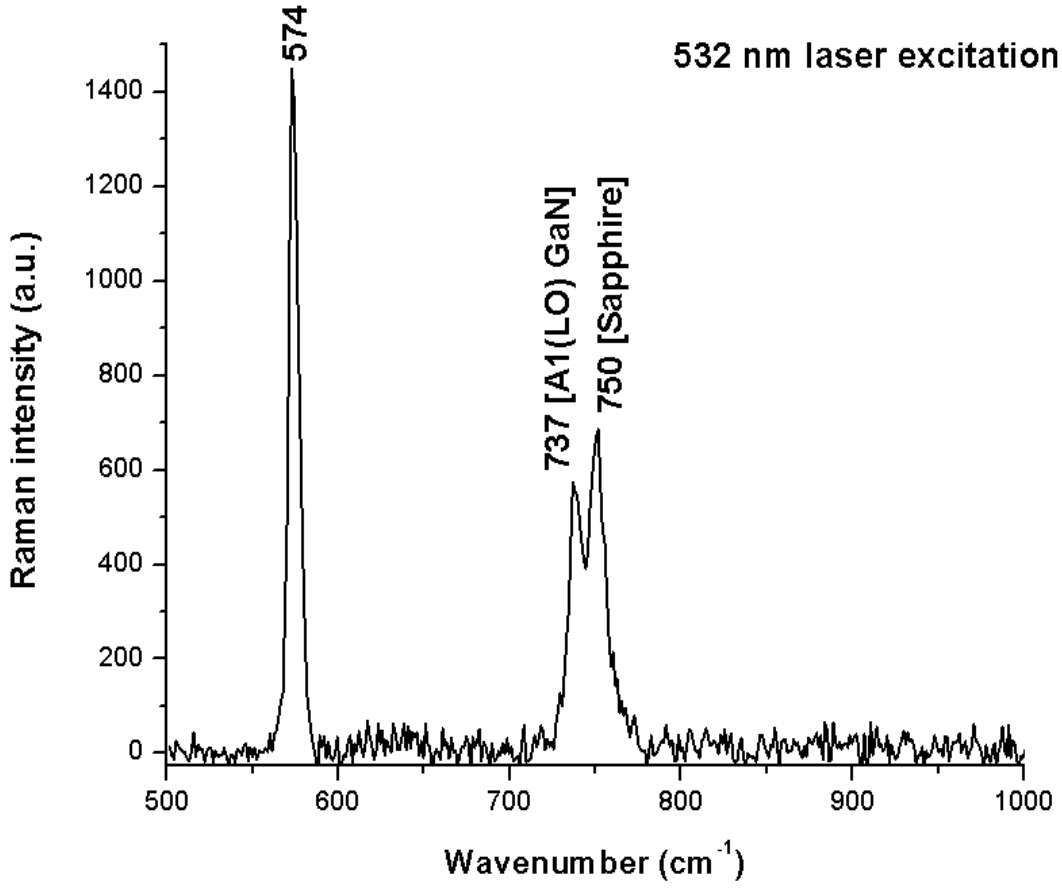

Figure 7. Raman spectra of AlN/GaN control wafer (Parameters: 20s exposure time, 1% Laser power.)

In related Raman results, we have also studied the temperature shifts in phonon spectra as in Ref. 38.

Summary

In this research, we have: determined the role of dimensional confinement on the lifetime of selected phonon modes; demonstrated that quantum wells may be realized that preferentially promote the emission of LO phonons in high-velocity interface phonon channels as opposed to lower-velocity confined phonons; demonstrated Raman-based techniques for measuring in semiconductors; formulated models for determining phonon dispersion curves and Frohlich potentials for multi-interface III-nitride heterostructures; and have made significant progress in

understanding the basic coupling of optical and acoustic phonons in dimensionally-confined wurtzite heterostructures.

References

1. R. Fuchs, K. L. Kliewer, and W. J. Pardee, Optical Properties of an Ionic Crystal Slab, Physical Review, 150, 589 (1966).
2. J. J. Licari and R. Evrard, Electron-phonon Interaction in a Dielectric Slab: the effect of the Electronic Polarizability, Phys, Rev. B, 15, 2254 (1977).
3. Michael A. Stroscio and Mitra Dutta, Phonons in Nanostructures, (Cambridge University Press, Cambridge, 2001), ISBN: 0521792797; also published in a Russia Language Edition by Dauka Press (2006) and in a Chinese Language Edition, Beijing (2005). This book presents dielectric continuum models as well as elastic continuum models for optical and acoustic phonon and demonstrates the utility of these models down to the nanoscale. Importantly, this book formulates these models for wurtzites – based on the original works of the authors and shows how to reduce the wurtzite treatment to the zincblende case. This last feature is especially important in the current proposal where we propose to generalize Cardona's equations to the case of wurtzites.
4. F. Comas, C. Trallero-Giner and M. Cardona, Continuum Treatment of Phonon Polaritons in Semiconductor Heterogeneous Structures, Physical Review B, 56, 4115 (1997).
5. B. C. Lee, K. W. Kim, M. Dutta and M. A. Stroscio, Electron-Optical-Phonon Scattering in Uniaxial Crystals, Phys. Rev., B56, 997 (1997).
6. B. C. Lee, K. W. Kim, M. A. Stroscio, and M. Dutta, Optical Phonon Confinement and Scattering in Wurtzite Heterostructures, Phys. Rev., B58, 4860 (1998).
7. S. M. Komirenko, K. W. Kim, M. A. Stroscio, and M. Dutta, Dispersion of Optical Phonons in Wurtzite Quantum Wells, Phys. Rev., B59, 5013 (1999).
8. S. M. Komirenko, K. W. Kim, M. A. Stroscio, and M. Dutta, Energy- Dependent Electron Scattering via Interaction with Optical Phonons in Wurtzite Crystals and Quantum Wells, Phys. Rev., B61, 2034 (2000).
9. S. M. Komirenko, K. W. Kim, V. A. Kochelap, and M. A. Stroscio, Runaway Effects in Nanoscale Group-III-Nitride Semiconductors, Physical Review, B64, 113207 (2001).
10. K. J. Nash, Electron-phonon Interactions and Lattice Dynamics of Optic Phonons in Semiconductor Heterostructures, Physical Review B, 46, 7723 (1992).

11. B. A. Auld, Acoustic Fields and Waves in Solids, Wiley Interscience Publication (John Wiley and Sons, New York, 1973).

12. C. Trallero-Giner, F. Garcia-Moliner, V.R. Velasco, and M. Cardona, Analysis of the Phenomenological Models for Long-wavelength Polar Optical Modes in Semiconductor Layered Systems, Physical Review B, 45, 11,944 (1992).

13. Banani Sen, Michael Stroscio, and Mitra Dutta, Piezoelectricity in wurtzite polar semiconductor nanowires: A theoretical study, J. Appl. Phys. 110, 024506 (2011); doi: 10.1063/1.3603036

14. Chen Chen, Mitra Dutta, and Michael A. Stroscio, "Electron Scattering via Interactions with Optical Phonons in Würtzite Crystals," Phys. Rev., B70, 075316-1-7, 2004.

15. Klemens P G 1966 Anharmonic decay of optical phonons *Physical Review* **148(2)** 845.

16. Barman S and Srivastava G P 2002 Lifetime of nonequilibrium zone-center longitudinal optical phonons in zinc-blende materials *Applied Physics Letters* **81(18)** 3395-3397.

17. Bhatt A R, Kim K W and Stroscio M A 1994 Theoretical calculation of longitudinal-optical-phonon lifetime in GaAs *Journal of Applied Physics* **76(6)** 3905-3907.

18. Vallée F and Bogani F 1991 Coherent time-resolved investigation of LO-phonon dynamics in GaAs *Physical Review B* **43(14)** 12049.

19. Ridley, B. K., 1996. The LO phonon lifetime in GaN. Journal of Physics: Condensed Matter 8(37) L511.

20. Yu S, Kim K W, Stroscio M A and Iafrate G J 1995 Electron–acoustic-phonon scattering rates in cylindrical quantum wires *Physical Review B* **51(7)** 4695.

21. Sarma S D, Campos V B, Stroscio M A and Kim K W 1992 Confined phonon modes and hot-electron energy relaxation in semiconductor microstructures *Semiconductor Science and Technology* **7(3B)** B60.

22. Ramayya E B, Vasileska D, Goodnick S M and Knezevic I 2008 Electron transport in silicon nanowires: The role of acoustic phonon confinement and surface roughness scattering *Journal of Applied Physics* **104(6)** 063711.

23. Balandin A and Wang K L 1998 Significant decrease of the lattice thermal conductivity due to phonon confinement in a free-standing semiconductor quantum well *Physical Review B* **58(3)** 1544.

24. Li X Q and Arakawa Y 1998 Anharmonic decay of confined optical phonons in quantum dots *Physical Review B* **57(19)** 12285.

25. Dyson, A. and Ridley, B.K., 2011. The lifetime of optical phonons in a single heterostructure *Journal of Applied Physics* **109(5)** 54509.

26. Cuffe J et al. 2013 Lifetimes of confined acoustic phonons in ultrathin silicon membranes *Physical review letters* **110(9)** 095503.

27. Kwon S, Wingert M C, Zheng J, Xiang J and Chen R 2016 Thermal transport in Si and Ge nanostructures in the 'confinement' regime *Nanoscale* **8(27)** 13155-13167.

28. Seitz F and Turnbull D 1958 *Solid state physics* (Vol. 7) Academic Press 19-21.

29. Verma P, Abbi S C and Jain K P 1995 Raman-scattering probe of anharmonic effects in GaAs *Physical Review B* **51(23)** 16660.

30. Born M and Huang K 1954 *Dynamical theory of crystal lattices* Clarendon press.

31. Stroscio M A and Dutta M 2001 *Phonons in Nanostructures* Cambridge University Press.

32. Bannov N, Aristov V, Mitin V and Stroscio M A 1995 Electron relaxation times due to the deformation-potential interaction of electrons with confined acoustic phonons in a free-standing quantum well *Physical Review B* **51(15)** 9930.

33. Bannov N, Mitin V and Stroscio M A 1994 Confined acoustic phonons in a free-standing quantum well and their interaction with electrons *physica status solidi (b)* **183(1)** 131-142.

34. Ahmed Mohamed, Kihoon Park, Can Bayram, Mitra Dutta, and Michael A. Stroscio, Confined and Interface Optical Phonon Emission in GaN/InGaN Double Barrier Quantum Well Heterostructures, PLoS ONE, 14(4): e0214971 https://doi.org/10.1371/journal.pone.0214971 1-12 PONE-D-19-02678R1 (May 2019).

35. Ketaki Sarkar, Debopam Datta, David J Gosztola, Fengyuan Shi, Alan Nicholls, Michael A Stroscio and Mitra Dutta, "Raman analysis of phonon modes in a short period AlN/GaN superlattice", Superlattices & Microstructures, 115, 116-122 (2018).

PAPERS PUBLISHED

Archival Publications (published) during reporting period:

Peer-reviewed papers:

Debopam Datta, Mitra Dutta, and Michael A. Stroscio, 2017, July. Coupled acousto-optical phonons in wurtzites: Micro-to-nano-scale bridging. In Nanotechnology (IEEE-NANO), 2017 IEEE 17th International Conference on (pp. 189-192). IEEE. DOI: 10.1109/NANO.2017.8117416

K. Park, M. A. Stroscio, and C. Bayram, Investigation of Electron Mobility and Saturation Velocity Limits in Gallium Nitride using Uniaxial Dielectric Continuum Model, Journal of

Applied Physics, 121(24), 245109-1-8 (2017). With UIUC - both Programs (UIUC and UIC) under the direction of Dr. Kenneth Goretta

Ketaki Sarkar, Debopam Datta, David J Gosztola, Fengyuan Shi, Alan Nicholls, Michael A Stroscio and Mitra Dutta, "Raman analysis of phonon modes in a short period AlN/GaN superlattice", Superlattices & Microstructures, 115, 116-122 (2018).

Debopam Datta, Kirupavathi Krishnababu, Michaal Stroscio, and Mitra Dutta, Effect of quantum confinement on lifetime of anharmonic decay of optical phonons in semiconductor nanostructures, Journal of Physics-Condensed Matter, 30(35), (2018) doi: 10.1088/1361-648X/aad104

Kihoon Park, Ahmed Mohamad, Can Bayram, Mitra Dutta, and Michael A. Stroscio, Electron Scattering via Interface Phonons with High Group Velocity in a Wurtzite GaN-based Quantum Well Structure, Nature Scientific Reports, 8, 15947 (2018) DOI: 10.1038s41598-018-34441-4 for publication, 2018).

Ahmed Mohamed, Kihoon Park, Can Bayram, Mitra Dutta, and Michael A. Stroscio, Confined and Interface Optical Phonon Emission in GaN/InGaN Double Barrier Quantum Well Heterostructures, PLoS ONE, 14(4): e0214971 https://doi.org/10.1371/journal.pone.0214971 1-12 PONE-D-19-02678R1 (May 2019).

Ahmed Mohamed, Mitra Dutta, and Michael A. Stroscio, Phonon Engineering to Modify Acoustic Phonon Velocity in Hexagonal Layered Superlattices, IEEE Electron Devices accepted May 2019.

Peer-reviewed proceeding summaries:

Debopam Datta, Kirupavathi Krishnababu, Michael A. Stroscio, Mitra Dutta, Effect of quantum confinement on lifetime of anharmonic decay of optical phonon in AlAs/GaAs/AlAs, The International Workshop on Computational Nanotechnology Conference, June 6-9, 2017, Windemere, UK Peer-reviewed Proceedings

Kihoon Park, Michael A. Stroscio, and Can Bayram, "Electron momentum relaxation rates via Frohlich interaction with polar-optical-phonons in bulk wurtzite gallium nitride" The International Workshop on Computational Nanotechnology Conference, June 6-9, 2017, Windemere, UK With UIUC - both Programs (UIUC and UIC) under the direction of Dr. Kenneth Goretta

Debopam Datta, Mitra Dutta, and Michael A. Stroscio, Coupled-Optical Phonons in Wurtzites: Micro-to-Nano-Scale Bridging, IEEE NANO 2017, Pittsburgh (July 2017). Peer-reviewed

Additional portions of these results were reported in presentation to AFRL:

Michael A. Stroscio, Mitra Dutta, Ramji Singh, Mojgan Mazouchi, Debopam Datta, Ahmed Mohamad, Ketaki Sarkar, Ke (Clare) Sun, Arash Darbandi, Kihoon Park, Can

Bayram, Continuum Models of Phonons in Nanostructures: Confined Phonon Effects in Heterostructure Devices, AFRL, July 2, 2018.

List of All Participating Scientific Personnel

Michael A. Stroscio, Co-PI
Mitra Dutta, PI
Michael A. Stroscio, Co-PI
Debopam Datta
Ketaki Sarkar
Ahmed Mohamed
Shreya Ghosh

Honors and Awards

The Co-PI was:

Chaired University Distinguished Professor Panel (2017); typically 3 or 4 UIC professors are selected each year.

Reappointed as the Richard and Loan Hill Professor (2017)

Award for Excellence in Teaching (2017) - typically 3 or 4 UIC professors are selected each year. This is UIC's highest teaching award.

Elected to the College of Fellows, American Institute of Medical and Biomedical Engineers

Report of Inventions: An invention Disclosure was filed on Reduction of Nitride-based Hotspot Temperature based Enhanced Generation of Fast Interface Phonons by Ahmed Mohamed [1], Kihoon Park [2], Can Bayram [2], Mitra Dutta [1], Michael Stroscio[1]

[1] Department of Electrical and Computer Engineering, University of Illinois at Chicago

[2] Department of Electrical and Computer Engineering, University of Illinois at Urbana-Champaign